LBL-12950

RECEIVED BY TIC AUG 26 1981

Lawrence Berkeley Laboratory
UNIVERSITY OF CALIFORNIA

CONF-8105104--4

MASTER

Presented at the Fifth High Energy Heavy Ion Summer Study, Lawrence Berkeley Laboratory, University of California, Berkeley, CA, May 18-22, 1981

WHAT CAN WE LEARN FROM INCLUSIVE SPECTRA?

Shoji Nagamiya

May 1981

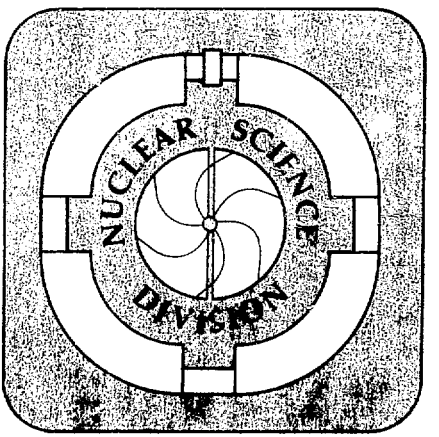

Prepared for the U.S. Department of Energy under Contract W-7405-ENG-48

LBL-12956

WHAT CAN WE LEARN FROM INCLUSIVE ? ?TRA?

Shoji Nagamiya

May 1981

Nuclear Science Division
Lawrence Berkeley Laboratory
University of California
Berkeley, CA 94720

This work is supported by the Director, Office of ...rgy Research, Division of Nuclear Physics of the Office of High-Energy and Nuclear Physics of the U.S. Department of Energy under Contract No. ...-7405-ENG-48.

WHAT CAN WE LEARN FROM INCLUSIVE SPECTRA?

Shoji Nagamiya

Nuclear Science Division, Lawrence Berkeley Laboratory
University of California, Berkeley, CA 94720

WHAT CAN WE LEARN FROM INCLUSIVE SPECTRA?

Shoji Nagamiya

Nuclear Science Division, Lawrence Berkeley Laboratory,
University of California, Berkeley, CA 94720

1. INTRODUCTION

I was asked to give a review at this Conference on the existing data of single particle inclusive spectra. Before I discuss this subject I would like to show one picture in Fig. 1 which was taken by a streamer chamber.[1] Here more than 50 charged particles are observed. In such a case it seems hopeless to learn anything meaningful from the detection of only one particle out of more-than-50. In the first place, therefore, I would like to point out that there is a certain limitation in physics which we can extract from single particle inclusive data.

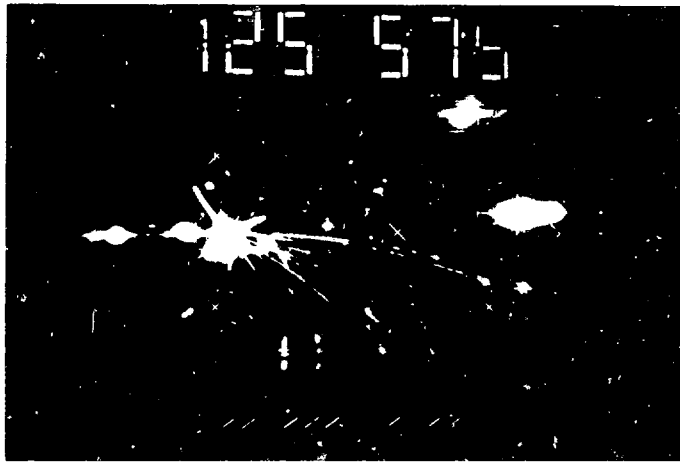

Fig. 1 An example of the streamer chamber picture of nuclear collision.

However, in Japan and China, there is an adage which says

一を聞いて十を知る (Hearing 1, you must learn 10; Japan)

举一反三 (Hearing 1, you must learn 3; China)

I don't know why 10 is decreased down to 3 in China.[2] Anyway, I would like to try to extract as much information as possible from the available data.

The organization of my talk is as follows.*) First I will describe very briefly the present experimental status on single particle inclusive measurements (Sec. 2). Then, I discuss the geometrical aspect of the collision from the data of total integrated cross sections of nuclear charge or mass (Sec. 3). The dynamical aspect of the collision, especially that for the participant region, forms the major part of my talk, and it will be discussed in connection with proton spectra (Sec. 4), composite fragment spectra (Sec. 5), pion production (Sec. 6), ratios of π^-/π^+, n/p and t/^{3}He (Sec. 7), and production of strange particles (Sec. 8). Then, I will describe the spectator physics from the data on projectile fragments (Sec. 9), and finally give a summary (Sec. 10).

2. CURRENT EXPERIMENTAL STATUS

So far a large number of experimental groups at the Bevalac have measured protons, neutrons, nuclear fragments and mesons at various kinematical regions. For example, the available proton and neutron data already cover a fairly wide kinematical region in the plane of rapidity (y) and transverse momentum (p_T/mc), as shown in Fig. 2. If the cross section is normalized to 1 in the projectile or target fragmentation region, the measured

*) In the actual presentation in the Conference I skipped Secs. 3, 4, and 7.

cross sections extend down to $10^{-(5-6)}$ which is about 10-100 $\mu b/sr/(GeV/c)^3$. However, I would like to point out also that the area allowed by the kinematics in the $y-p_T/mc$ plane is still much wider than the area covered by the available data. With a reasonable experimental device we can measur· the cross section down to 10^{-10} at the Bevalac. Such measurements of small cross sections are definitely important in the near future.

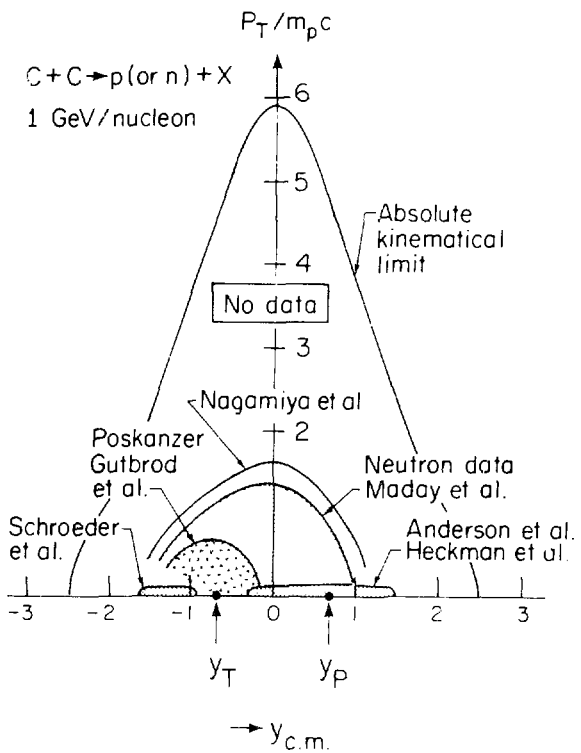

XBL816-2355

Fig. 2 Current experimental status for measurements of protons and neutrons.

A similar situation is observed for pion measurements, as shown in Fig. 3. Data are available over a fairly wide kinematical region, but still there is a wide region over which the cross sections have not yet been measured. In the near future we should try to measure cross sections down to 1 nb/sr/(GeV/c)^3.

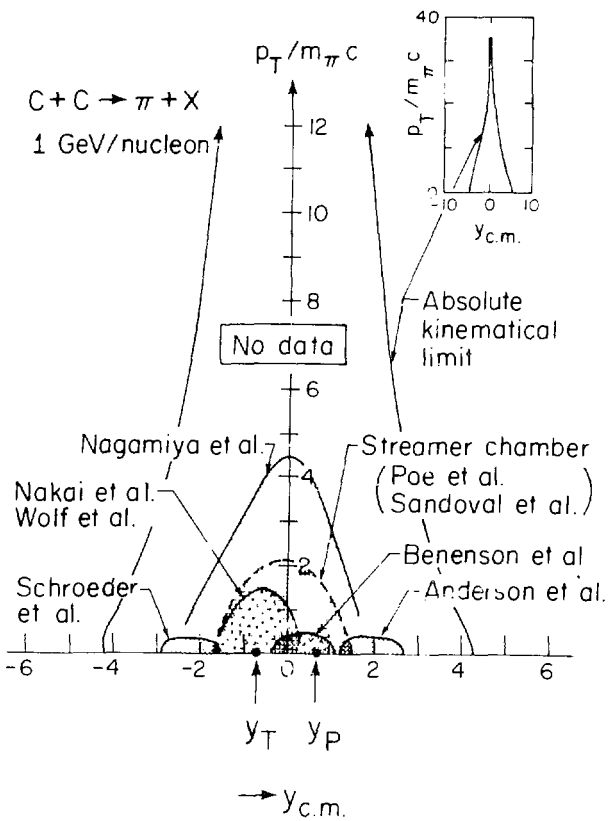

XBL 816-2356

Fig. 3 Current experimental status for measurements of pions.

3. TOTAL INTEGRATED CROSS SECTIONS OF NUCLEAR CHARGE OR MASS

In high energy nuclear collisions it has been rather well known that the participant-spectator model[3] explains gross features of the emission of nuclear fragments including protons and neutrons. For example, a large fragment yield at $(y,p_T) \approx (y_p,0)$ or $(y_T,0)$ is mainly due to the spectator while the smooth proton or pion spectra at large angles are primarily due to the participant. By using this model we first calculate how many protons (nucleons) are classified as participant protons (nucleons) and how many are as spectator protons (nucleons).

Let us assume that the projectile nucleus consists of Z_p protons and N_p neutrons (and therefore, $A_p = Z_p + N_p$), and similarly assume that the target nucleus consists of A_T nucleons. Then, the average number of participant protons from the projectile nucleus, which represents the participant charge from the projectile, is given by Z_p times the target cross section divided by the total geometrical cross section, because projectile protons which hit the target are regarded as participant protons. We thus have

$$\langle Z_{Proj}^{Parti} \rangle = Z_p \times (\text{Target cross section})/\sigma_0$$

$$= Z_p A_T^{2/3}/(A_p^{1/3} + A_T^{1/3})^2, \qquad (1)$$

where σ_0 is the total cross section which is approximately given by

$$\sigma_0 = \pi r_0^2 (A_p^{1/3} + A_T^{1/3})^2. \qquad (2)$$

Similarly for the average number of participant protons from the target nucleus we have

$$\langle Z_{Targ}^{Parti} \rangle = Z_T A_p^{2/3}/(A_p^{1/3} + A_T^{1/3})^2. \qquad (3)$$

The total integrated yield of participant protons, namely the total

integrated yield of nuclear charge from the participant region, is the sum of the above participant proton numbers multiplied by the total cross section σ_0, and is given by

$$\sigma_{tot}^{charge}(\text{Participant}) = (\langle Z_{Proj}^{Parti} \rangle + \langle Z_{Targ}^{Parti} \rangle) \times \sigma_0$$

$$= \pi r_0^2 \, (Z_P A_T^{2/3} + Z_T A_P^{2/3}). \qquad (4)$$

Similarly for the total integrated cross sections of nuclear charge for projectile and target spectators we have

$$\sigma_{tot}^{charge}(\text{Proj Frag}) = (Z_p - \langle Z_{Proj}^{Parti} \rangle) \times \sigma_0$$

$$= \pi r_0^2 \, Z_p (A_P^{2/3} + 2A_P^{1/3} A_T^{1/3}), \qquad (5)$$

$$\sigma_{tot}^{charge}(\text{Targ Frag}) = \pi r_0^2 \, Z_T (A_T^{2/3} + 2A_P^{1/3} A_T^{1/3}). \qquad (6)$$

These formulas are the natural consequence of the Glauber theory[4] and have been derived also in Refs. 5 and 6. For A + A collisions with Z = N we should note that the above values of σ in Eqs. (4)-(6) are proportional to $A^{5/3}$. This value of 5/3 for the power dependence is referred to as the geometrical limit.

In Figs. 4-6 the above three formulas are compared with data. Shown in Fig. 4 are the values of σ_{tot}^{charge} measured by Lindstrom et al.[7] for C and O projectiles. First we notice that the yields are almost independent of the beam energy. Secondly, the observed yields are approximately proportional to $A_T^{1/4}$. Thirdly, the absolute values of σ_{tot}^{charge} are very well explained by Eq. (5) with r_0 = 0.95 fm. When these data were published, it was thought that the observed $A_T^{1/4}$ dependence showed evidence that projectile fragments are produced mostly from "peripheral" collisions. However, this conclusion is not obvious, because the participant-spectator model does not specify any impact

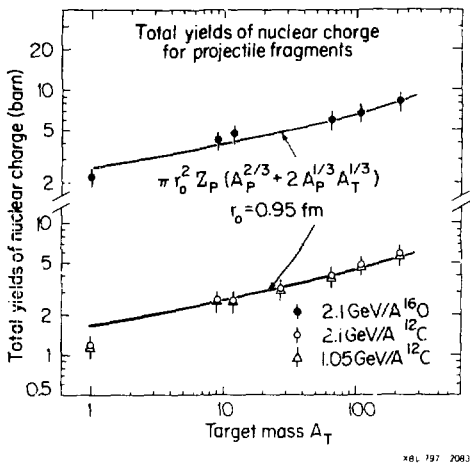

Fig. 4 Total integrated cross sections of nuclear charge for projectile fragments as compared with Eq. (5).

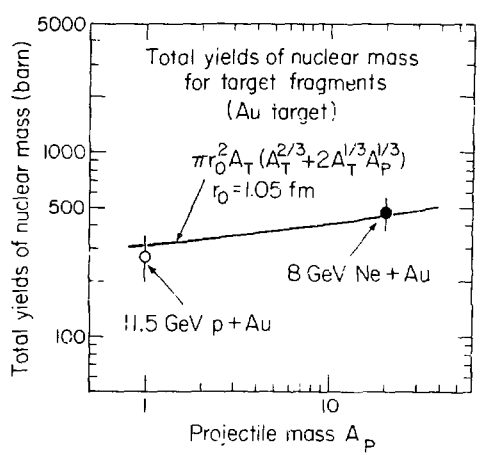

Fig. 5 Total integrated cross sections of nuclear mass for target fragments as compared with Eq. (6).

parameter, and some projectile fragments can be produced even from small impact parameters. Still, this model predicts approximately the $A_T^{1/4}$ dependence due to the existence of the $A_p^{2/3}$ term which is added to the term of $2A_p^{1/3}A_T^{1/3}$ in Eq. (5).

A similar plot for target fragments is shown in Fig. 5. Here, the total integrated cross sections of nuclear mass in the two collisions, 11.5 GeV p + Au (Ref. 8) and 400 MeV/nucleon Ne + Au (Ref. 9), are plotted. The data are again explained by Eq. (6) with r_0 = 1.05 fm [Note that in this case we should replace Z_T by A_T in Eq. (6), since we plot the total mass yields instead of the total nuclear charge yields].

Fig. 6 shows the sum of charges for p, d, t, and ^{3}He evaluated from the relatively high-energy fragment data observed at large angles.[10] These data

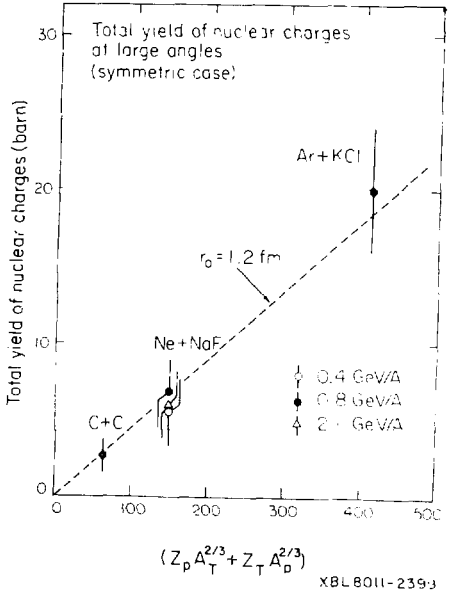

Fig. 6 Total integrated cross sections of nuclear charge for the participant region as compared with Eq. (4).

should now be compared with Eq. (4), since most of such fragments are expected to originate from the participant. We again observe that the total integrated cross sections are almost independent of the beam energy, and the agreement of the data with Eq. (4) is good if we take $r_0 = 1.2$ fm.

SUMMARY:

1. The total integrated cross sections of nuclear charge or mass are almost independent of the beam energy. The observed absolute values of cross sections are well explained by the participant-spectator model. Thus, the total integrated cross sections are determined largely by the collision geometry only.
2. The observed $A_T^{1/4}$ dependence of the cross section for the projectile fragments can be explained by the participant-spectator model, and thus, this power dependence does not immediately imply that projectile fragments are produced from peripheral collisions.
3. The value of r_0 for the participant region ($r_0 \approx 1.2$ fm) is larger than that for the region of projectile or target fragmentation ($r_0 \approx 1.0$ fm), implying that the clean-cut participant-spectator model might not be appropriate to describe the details of the collision geometry. Some nucleons which are located in the boundary region would carry an intermediate nature between the participant and spectator. In the present analysis these intermediate nucleons are probably counted as participant.

4. PROTON SPECTRA

Once we understand the geometry, the next immediate interest is the collision dynamics. Since the spectator part does not experience any violent nucleon nucleon interaction, the most interesting region from the viewpoint of the reaction mechanism is the participant part. I will therefore discuss the

the participant dynamics from this section through to Sec. 8. Physics related to the spectator will be described in Sec. 9.

So far a large number of proton data have been reported.[10-15] Since these data have been frequently mentioned in several conferences, I will skip most of them in the present talk and show only one piece of the data. Shown in Fig. 7 are the proton energy spectra at c.m. 90°, which corresponds to $y = (y_p + y_T)/2$, from three sets of nearly equal-mass nuclear collisions, C + C, Ne + NaF, and Ar + KCl.[13,10] Here the invariant cross sections, σ_{inv},

$$\sigma_{inv} \equiv E(d^3\sigma/d^3p) \tag{7}$$

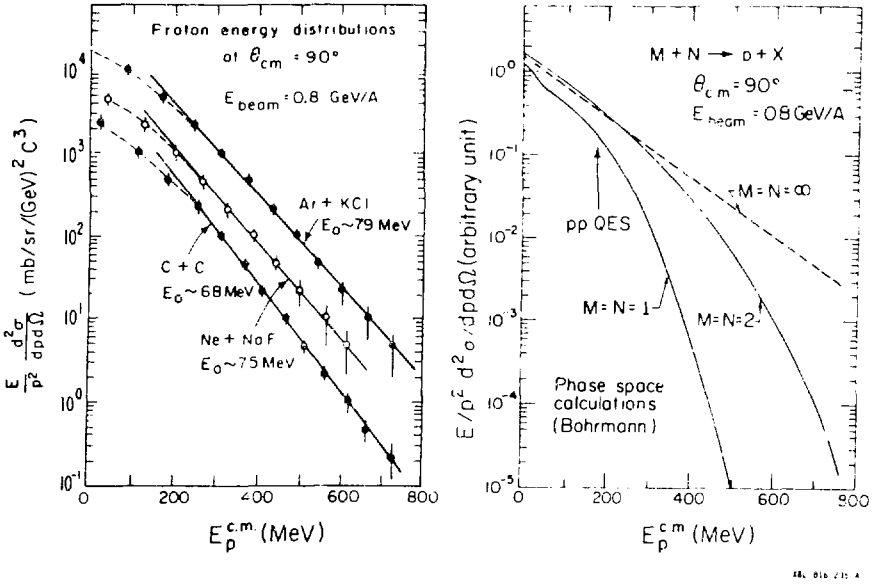

Fig. 7 Proton energy spectra at θ(c.m.) = 90° measured in collisions of 800 MeV/nucleon C + C, Ne + NaF, and Ar + KCl (left), and the phase space calculation of the proton emission at 800 MeV/nucleon done by Bohrmann (right). Fermi motion as well as elastic and inelastic processes are included in the calculation.

are plotted as a function of the kinetic energy, $E_p^{c.m.}$. The nominal beam energy was 800 MeV/nucleon for all cases. These data tend to reflect more of the features of the participant region, because at $\theta_{c.m.} \approx 90^o$ the influence from the spectator is the smallest.

First we notice that the spectrum shape is almost identical for the three collisions. This fa t implies that the beam energy per nucleon rather than the total beam energy plays a key role in determining the collision dynamics. Secondly, the spectrum shape approaches an exponential at high energies but it deviates substantially from the exponential shape at low energies. Such a "shoulder arm" type distribution is a typical feature seen in the proton spectra at 800 MeV/nucleon. The turning point between the shoulder and arm sits at around $E_p^{c.m.} \approx 200$ MeV, which is very close to the projectile (or target) energy per nucleon in the c.m. frame (182 MeV in this case). This fact implies that protons from quasi-elastic pp or pn scatterings might be responsible for creating such a turning point.

In order to study these observed spectra in more detail I show in Fig. 7 a phase-space calculation by Bohrmann.[16] If we consider the case in which a nucleus-nucleus collision is a simple incoherent sum of single NN collisions without any succeeding multiple collisions, then two nucleons, one from the projectile and the other from the target, determines the whole dynamics. As shown in the M = N = 1 system in Fig. 7, the spectrum in this case has a rather clear turning point at around $E_p^{c.m.} \approx 182$ MeV (indicated by pp QES in the figure). This spectrum, however, is quite different from the observed one, especially in the high ener region. If multiple NN collisions take place, then the available energy tends to be shared among larger number of nucleons than two, and the yields of high energy protons could increase. In fact, if four nucleons, two from the projectile and two f m the target, share the available energy, then the shape of the calculated spe rum drastically

changes at high energies, and the calculated spectrum becomes much closer to the observed one. The extreme limit of multiple NN collisions is the thermal case in which we have an almost pure exponential shape which disagrees with the data. Therefore, the observed spectrum indicates that both the single and multiple NN collision processes are important, and especially the latter in the region of the high energy tails.

The importance of multiple NN collisions in producing the high energy tails is observed also in data on the A dependence. For nearly equal mass collisions the observed cross sections shown in Fig. 7 are parameterized, to a good approximation, by

$$\sigma_{inv}(E_p^{c.m.}) \propto A^{\alpha}, \qquad (8$$

where A is the projectile (and target) mass. The observed values of α are displayed in Fig. 8 for various c.m. kinetic energies, $E_p^{c.m.}$. For low energy

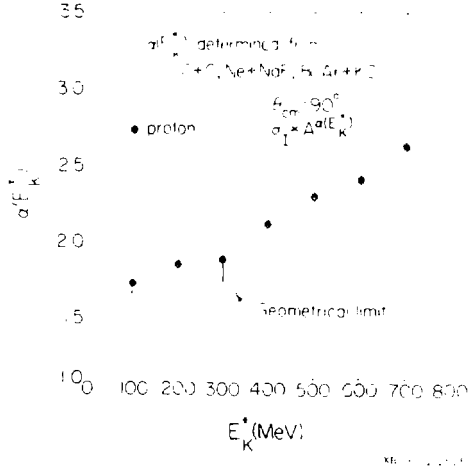

Fig. 8 A dependence of proton emission in A on A collisions.

protons we observe $\alpha \approx 5/3$ which is the geometrical limit mentioned in the previous section. For high energy protons, however, α is substantially larger than this geometrical limit. A larger power than 5/3 implies that more nucleons are involved in a collision than geometrically expected, which is possible through multiple NN collisions. Therefore, these data strongly suggest the importance of the multiple NN collisions for the production of high energy protons at c.m. 90°, or in other words, for the production of high p_T protons.

The reason why I mention such classical data is because I would like to remind you again the importance of both "direct" and "multiple-collision" components in particle production in high energy nuclear collisions. Although such a mixture of the two components has been clearly observed in the two proton correlation data,[17,13] some evidences of it are already observed in inclusive proton spectra. When the fireball model was proposed,[11] the fit to the data was done only for low energy protons below the per nucleon beam energy, since thermal protons tend to be of low energy. However, we now observe that low energy protons substantially deviate from the exponential shape and cannot be explained by any thermal model. The exponential shape is only valid at high energies where non-thermal particles are emitted. Here we find a dilemma of the thermal model.

SUMMARY:

1. The spectrum shape of protons at c.m. 90° at the beam energy of around 1 GeV/nucleon is characterized by the "shoulder-arm" shape.
2. The beam energy per nucleon (not the total beam energy) determines the major feature of proton emission.
3. The comparison of the observed spectra with a phase space calculation as well as the observed A dependence suggest the importance of the multiple NN collision process for the production of large p_T protons.

4. Low energy protons originate both from direct and multiple collisions. This was also confirmed by the two proton correlation experiment. In addition, the known experimental fact that $\lambda \approx R$ at the beam energy of 1 GeV/nucleon supports this conjecture, where λ is the nucleon mean free path inside the nucleus (which is about 2.4 fm[18]) and R is the size of the interaction region (which is 2-3 fm according to the discussion in Sec. 5.2.).

5. FORMATION OF COMPOSITE FRAGMENTS

5.1. Power Law

From the participant region protons and neutrons are emitted over a wide range of energy and angle. In this case there is a certain chance that these nucleons stick together to form a composite fragment. Naively we therefore expect that the probability of forming a deuteron at a velocity $\vec{v}_d$ is proportional to the product of the probabilities of finding a proton and a neutron at the same velocity:

$$P_d(\vec{v} = \vec{v}_d) \propto P_p(\vec{v} = \vec{v}_d) \cdot P_n(\vec{v} = \vec{v}_d). \qquad (9)$$

If neutron spectra can be replaced by proton spectra, then we expect the cross section of the composite fragment with mass number A to be given by,

$$E_A(d^3\sigma_A/d^3p_A) = C_A\,[E_p(d^3\sigma_p/d^3p_p)]^A, \qquad (10)$$

where $p_A = A \cdot p_p$, and C_A is a constant.

In Fig. 9 the spectra of deuterons[10] from 800 MeV/nucleon C + C collisions are shown and they are compared with the squares of the observed proton spectra. With one normalization constant C_A the above power law of Eq. (10) holds extremely well.

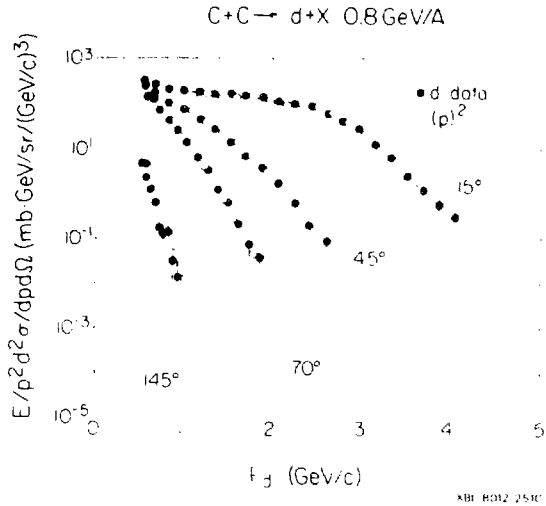

Fig. 9 Deuteron spectra as compared with the squares of proton spectra.

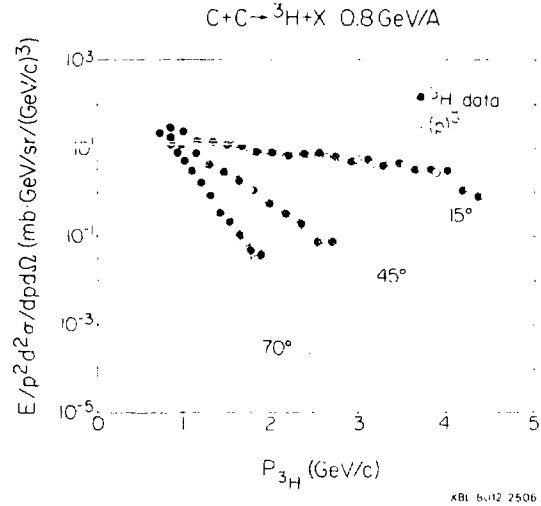

Fig. 10 Triton spectra as compared with the cubes of proton spectra.

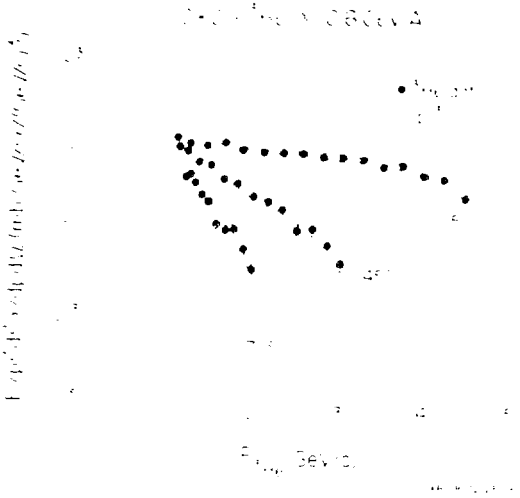

Fig. 11 ^{3}He spectra as compared with the cubes of proton spectra.

The triton spectra from the same reaction are shown in Fig. 10. In this case the spectra agree very well with cubes of the observed proton spectra. Similarly the power law holds very well for ^{3}He, as shown in Fig. 11, and of course, we expect nearly the same yields for tritons and ^{3}He from C + C collisions, as seen in Figs. 10 and 11.

Let us study in more detail the implication of this power law. In Fig. 13 I show the observed deuteron cross sections divided by the squares of the observed proton cross sections for Ne + U collisions at three bombarding energies, 400, 800, and 2100 MeV/nucleon.[10] The value C_A is almost independent of the deuteron momentum as well as the deuteron emission angle. In addition, the value C_A is almost independent of the projectile energy. What do we learn from these data?

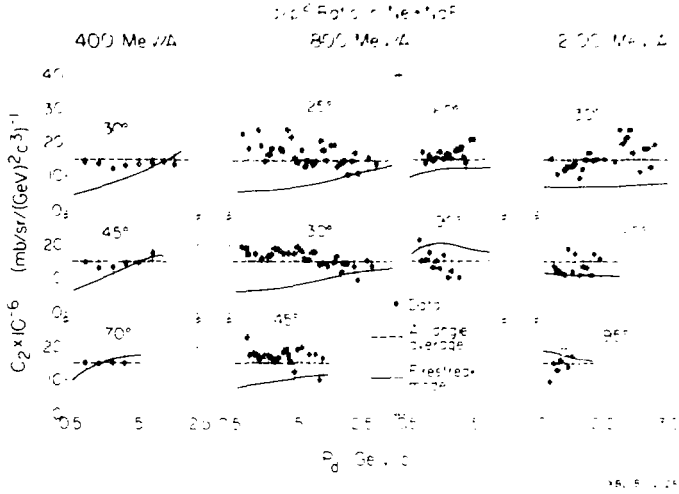

Fig. 12 Observed d/p^2 ratios for Ne + NaF collisions.

If the particle density in unit phase space volume is given by $f(\vec{p})$ such that

$$(1/V)\cdot/d^3n/d^3p) = f(\vec{p}), \tag{11}$$

then the ratio C_A is given by

$$C_A = (1/\gamma V)^{A-1}\cdot f(\vec{p}_A)/[f(\vec{p}_p)]^A \qquad \text{with } \vec{p}_A = A\cdot\vec{p}_p. \tag{12}$$

Now, what do we expect for C_A in terms of various models? In a simple fireball model[11] $f(\vec{p})$ is simply given by

$$f(\vec{p}) \propto e^{-E/T}. \tag{13}$$

Consequently, C_A is given by

$$C_A = \text{const.}/(\gamma V)^{A-1}, \tag{14}$$

where γ is the Lorentz factor of the emitted particle measured relative to the c.m. frame of the fireball.[19] In the data shown in Fig. 12 the range of γ is 1.0 - 1.3 for 400 MeV/nucleon, 1.0 -1.6 for 800 MeV/nucleon, and 1.1 - 2.0 for 2.1 GeV/nucleon. Therefore, within a factor two the simple thermal model agrees with the observed fact the C_A is almost constant.

However, it has been well known that the simple fireball model does not explain any data. Especially the large anisotropy of the observed angular distribution[10] in the c.m. frame cannot be explained by this model. In order to reproduce the angular anisotropy the firestreak model[20,21] was proposed and it has been often used to fit the data. In this model the nucleus is divided into several tubes in order to take into account the geometry more accurately than the simple fireball model. As a result, the temperature is different from tube to tube. Here, $f(\vec{p})$ is given by

$$f(\vec{p}) = \sum a_i e^{-E/T_i}, \tag{15}$$

and C_A is no longer constant but has a strong fragment-energy dependence. For example, the predicted value[21] of C_A in the case of 400 MeV/nucleon at 30^o (left upper corner in Fig. 12) changes from 5 to 20 which clearly disagrees with the data. Therefore, the firestreak model has trouble in reproducing the observed power law. This fact further indicates that the composite fragments may not be produced from a macroscopic chemical equilibrium inside the fireball.

In the coalescence model[22-25] nucleons which are located within a radius of p_0 in the momentum space stick together to form a composite fragment. In this case C_A is given by

$$C_A \propto [(4\pi/3)\cdot p_0^3]^{A-1}. \quad (16)$$

We should note, however, that in this model, if there are two or more nucleons inside the radius p_0, then the assembly of these nucleons is immediately regarded as a real composite particle. Therefore, the cross section of composite fragment A is expressed as

$$\sigma_A = C_A[\sigma(\text{original nucleon})]^A, \quad (17)$$

namely, the cross section of a composite fragment is proportional to the A^{th} power of the cross section of the original nucleons before the formation of

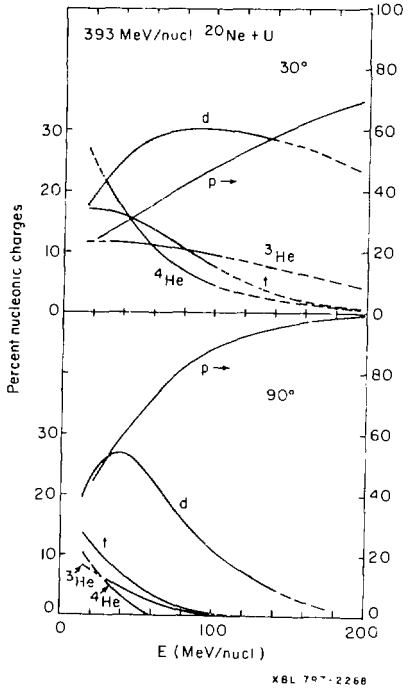

Fig. 13 Percentage fractions of nuclear fragments in 393 MeV/nucleon Ne + U.

composite fragments. However, the experimental fact is that the power law holds between observed cross sections:

$$\sigma_A(\text{observed}) = C_A[\sigma(\text{observed proton})]^A. \qquad (18)$$

Of course, if the observed proton cross sections are much larger than the observed cross sections of composite fragments, then there is no significant difference between Eqs. (17) and (18). But, as shown in Fig. 13, the yield ratios between composite particles and protons are sometimes comparable to each other in certain kinematical regions.[14] Still, the power law holds well between the observed composites and the observed protons. Therefore, when we apply the coalescence model, we have to assume that the local chemical equilibrium exists between the formation and break-up of composite fragment, such as $d \leftrightarrow p + n$. If the local chemical equilibrium holds, then why not the macroscopic chemical equilibrium? This is a very interesting subject which has to be studied in the future.

5.2. Size of the Interaction Region

Next, we discuss another aspect of the ratio C_A. As seen from Eq. (12), C_A is related to the phase space volume V or the radius R ($= (3V/4\pi)^{1/3}$). In Fig. 14 the radii obtained in various collisions at 800 MeV/nucleon[10] are shown. Here, the theoretical model of Mekjian[26] has been used. The observed radius increases as the projectile and target masses increase. Also, the radius increases as the mass of the detected composite fragments decreases. Why do we observe such features?

Recently Sato and Yazaki[27] proposed a theory to relate the observed radius R with the real source radius R_0 and the radius of the composite fragment R_A by the following formula:

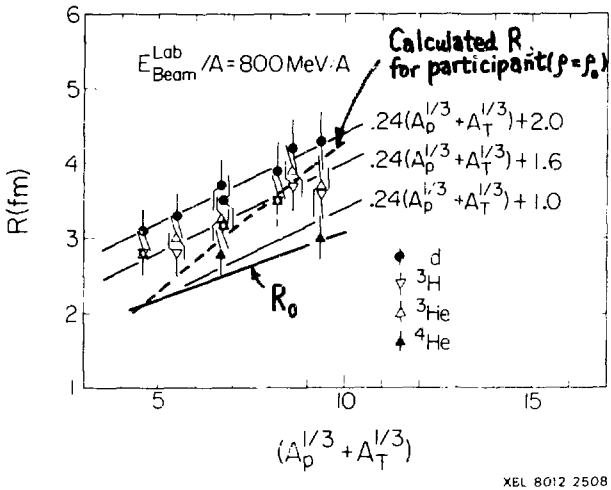

Fig. 14 The radius of the phase space volume determined from the observed power law. The formula of Mekjian is used. Also, the empirical source radius R_0 as well as the calculated R_0 are shown.

$$R \propto 1/p_0 = \kappa \times \sqrt{R_0^2 + R_A^2}. \tag{19}$$

At the present moment the predicted value of κ cannot be used to explain the whole set of available data, but qualitatively this formula explains the observed larger tendency that R is larger for lighter mass composite fragments, since the radius R_A is 2.2 fm for d, 1.7 fm for t and ^{3}He, and 1.3 fm for α, and thus monotonically decreases as the mass of the emitted fragment increases.

If we admit that the observed radius R is determined only by R_0 and R_A, then we can empirically evaluate R_0 by plotting the observed values of R^2 as a function of R_A^2 and by extrapolating R^2 to the limit of $R_A^2 = 0$. Such empirical values of R_0 are also shown in Fig. 14, which ranges from 2 to 3 fm. Also, in Fig. 14 the calculated values of R_0 based on the participant-spectator model are plotted for normal nuclear density ($\rho = \rho_0$). We observe good agreement

between the calculated and observed values for light mass systems such as C + C, whereas the calculated value is much larger than the observed one for heavy mass systems such as Ar + Pb. Of course, it is too early to say that this may be an evidence on the formation of high density, but it is certainly interesting to study in more detail the source radius from the composite spectra.

5.3. Entropy

So far I have discussed mainly the power law. A simple yield ratio between composite fragment and proton tells us another type of information.

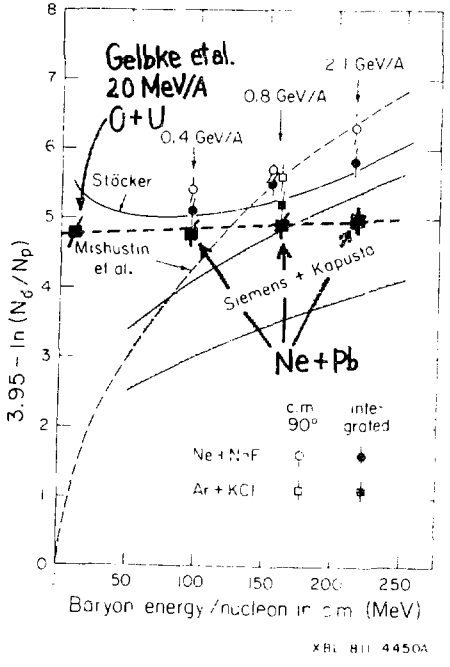

Fig. 15 The observed d/p ratio and the entropy.

One of the topics related to this yield ratio is the entropy. This discussion was initiated by the work of Siemens and Kapusta.[28] They pointed out two aspects. One is that the d/p ratio is related to the quantity of entropy, S, by the relation of

$$S = 3.95 - \ln(N_d/N_p), \tag{20}$$

and the other is that the observed entropy is much larger than the theoretical ent[illegible] Therefore, they thought that perhaps a new degree of freedom is created in high energy nuclear collisions.

In this Conference this subject of the entropy will be discussed at length by G. Bertsch[29] and H. Stöcker[30], and therefore I will not go into details in the present talk. Instead, I would like to point out three aspects related to this entropy work. The first point is that a new calculation by Mishustin et al.[31] who took into account the pion degree of freedom explains reasonably well the data except for that with 400 MeV/nucleon beams. The second point is that, if we plot the data for non-symmetric system such as Ne + Pb (Ref. 10) or O + U (Ref. 32), then the d/p ratio stays almost constant at all bombarding energies from 20 to 2000 MeV/nucleon. This fact implies that the d/p ratio may not be directly related to the quantity of entropy. In fact, Stöcker has recently shown that the observed d/p ratio has no relationship to the entropy, and has predicted the almost beam-energy independent d/p ratio, as shown in Fig. 15. The third point which is a more philosophical question, is the production mechanism of composite fragments. As mentioned previously, the macroscopic chemical equilibrium may not be the real production mechanism of composite fragments. The quantity of entropy is directly related to the chemical potential μ by the formula $S = 5/2 - \mu/T$, where T is the temperature. Therefore, unless it is proved that the macroscopic chemical equilibrium is the real production mechanism of composite

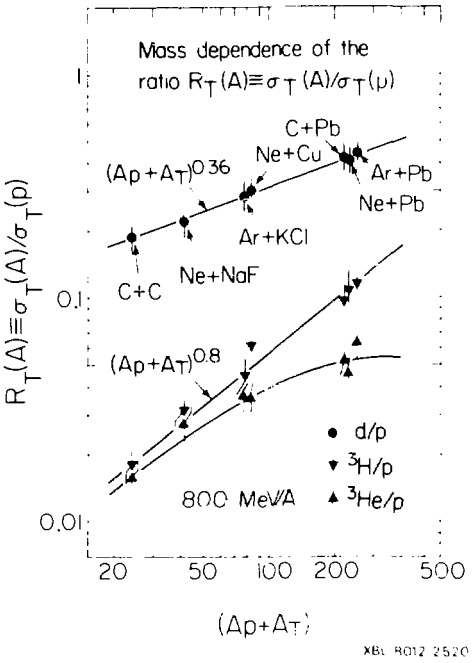

Fig. 16 Ratios of d/p, t/p and ^{3}He/p plotted as a function of the total mass number of the system.

formation, it is rather difficult at least for me to immediately accept the relationship between the entropy and the observed d/p ratio.

Finally I would like to point out the finite size effect of the system on the composite formation. In Fig. 16 the d/p ratios or t/p ratios are plotted as a function of the projectile mass plus the target mass.[10] Larger ratios are observed for heavier mass systems. This is understandable, because more combinations between nucleons are available for heavier mass systems. However, most of the theoretical models have not correctly treated this finite size effect of the system, and predict a constant yield ratio for any combination between the projectile and target.[33] This point has to be

correctly solved especially before discussing the entropy.

SUMMARY:

1. A power law given by Eq. (10) holds very well between the observed proton and composite-fragment spectra. If we use the coalescence model, we have to assume local chemical equilibrium between the formation and break-up.
2. The observed C_A is independent of beam energy as well as the fragment energy and angle, and depends only on the projectile and target masses. This fact is inconsistent with the prediction of the firestreak model and suggests that macroscopic chemical equilibrium may not be the mechanism responsible for producing composite fragments.
3. Source radii were derived from the observed values of C_A. The results are 2-3 fm, depending on the mass of the system.
4. With regard to the yield ratio between the composite particles and protons, all theoretical models should first consider the finite size effect of the system.
5. The discussion of the entropy is certainly interesting, but there is a question on the relationship between the d/p ratio and the entropy.

6. PION PRODUCTION

6.1. Multiplicity

For beam energies around 1 GeV/nucleon the dominant secondary particles created in the collisions are pions. In this section we review recent progress on pion production.

As an introduction I discuss the pion multiplicity. Since the total intergrated inclusive cross section, σ_{incl}^{tot} is given by

$$\sigma_{incl}^{tot} = \langle m \rangle \cdot \sigma_0, \qquad (21)$$

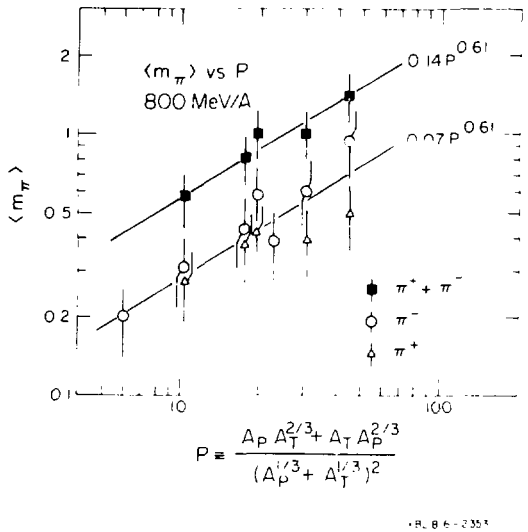

Fig. 17 Observed pion multiplicities $\langle m_\pi \rangle$.

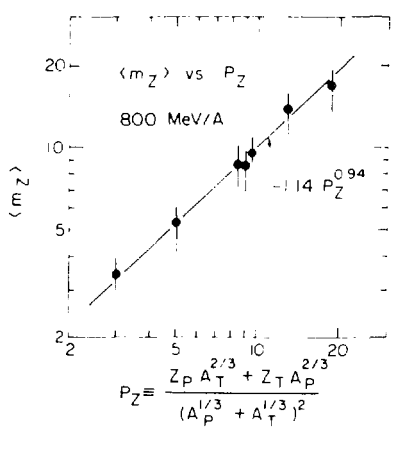

Fig. 18 Observed multiplicities of total nuclear charge, $\langle m_Z \rangle$.

where σ_0 is the total cross section, we can evaluate the average multiplicity <m> from the inclusive data. In Fig. 17 the observed values of $\langle m_\pi \rangle$ are plotted as a function of the average participant nucleon number, P, for various projectile and target combinations at 800 MeV/nucleon. The multiplicity is roughly parametererized as[34]

$$\langle m_\pi \rangle = a \cdot P^x, \tag{22}$$

with $x \approx 2/3$. This implies that the pions are emitted from the surface of the participant and not from deep inside the participant region. If we compare these data with the average multiplicity of total nuclear charge, $\langle m_Z \rangle$, the difference is much clearer. As seen in Fig. 18, the multiplicity $\langle m_Z \rangle$ increases almost linearly with the average participant proton number, P_Z. Therefore, the $P^{2/3}$ dependence of the pion multiplicity strongly suggests the importance of the pion absorption process. So far a number of theoretical models[21,35] have overestimated the pion yields, since they do not take into consideration the pion absorption effect. I would like to emphasize here that all the theoretical models should first include the pion absorption before they are compared with the data.

6.2. Energy and Angular Distributions

Then, how about the energy spectra? In Fig. 19 the energy distributions of negative pions at 0°, 180°, and at 90° are plotted in the c.m. frame. Data were taken with 2.1 GeV/nucleon beams, but unfortunately no direct comparison can be done for the same projectile and target combinations. An important message obtained from this figure is that the energy distribution is almost exponential at any emission angle. Also, the 0° and 180° data currently cover much wider kinematical regions than the 90° data.

In Fig. 20 the inverse exponetial slopes E_0 are plotted as a function of

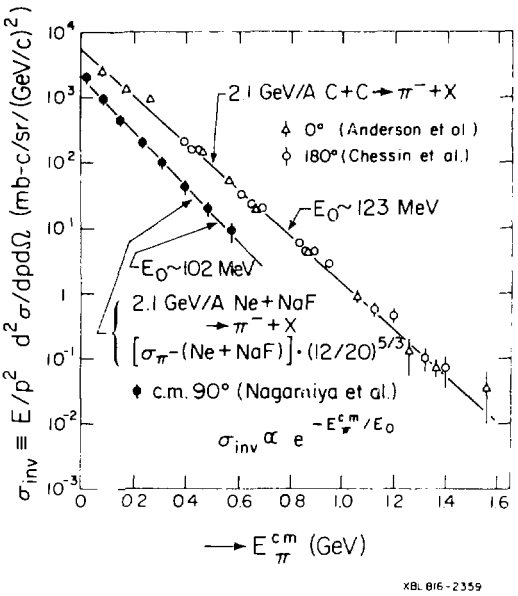

Fig. 19 Pion spectra at E_{Lab}^{Beam} = 2.1 GeV/nucleon.

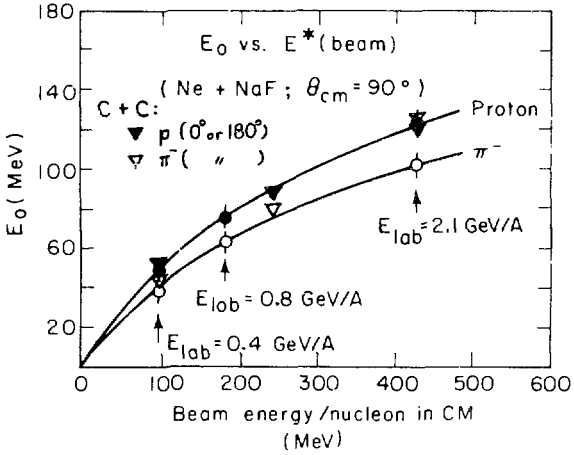

Fig. 20 Observed inverse slopes E_0 at 90° as compared with those at 0° and 180°.

the beam energy per nucleon in the c.m. frame. The value of E_0 monotonically increases with the beam energy. Also, the data at 0^o and 180^o show almost the same behavior with the data at 90^o except at E_{Lab} = 2.1 GeV/nucleon.[36]

Of course, there is no a priori reason that the spectrum shape should be exponential. In fact, Anderson et al.[37] showed that the energy distributions in the nucleon-nucleon c.m. frame are not exponential for proton and deuteron beams. For projectiles heavier than α the spectrum shape approaches exponetial, as shown in Fig. 21. In this figure we also observe that yields of high energy pions are significantly higher for heavier mass projectiles. This is an interesting feature and suggests cumulative effects.

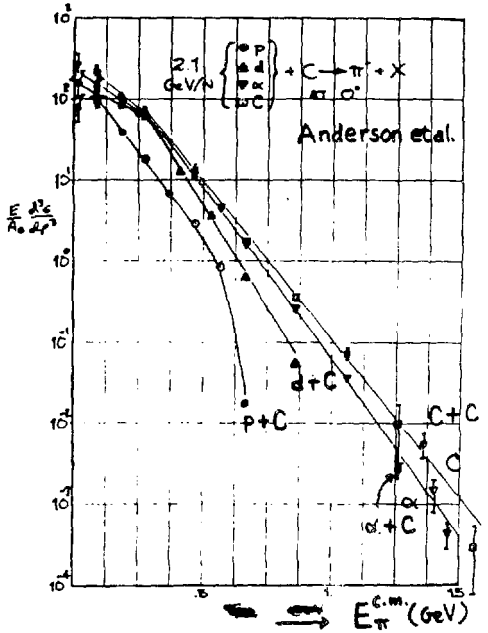

Fig. 21 Pion spectra by various projectiles at 2.1 GeV/nucleon.

Next I discuss the angular distribution. I discuss it for a beam energy of around 1 GeV/nucleon in Ar + KCl or Ar + Ca collisions. Shown in Fig. 23 are the ratios of the π^- cross sections between 30° and 90° in the c.m. frame for 800 MeV/nucleon Ar + KCl collisions, plotted as a function of the pion energy in that frame. The ratio has a peak at around $E_\pi^{c.m.} \simeq 150$ MeV. This observed feature has not yet been explained by any conventional theoretical model, but it seems that such a feature of pion emission is consistent with the expectation that most of the pions are from Δ_{33} resonances, since the decay from Δ increases the pion yield at around 150 MeV and might have a large anisotropy there.

Another interesting subject of the angular distribution is its detailed structure for low energy pions at $E_\pi^{c.m.} \simeq 10$-20 MeV. Wolf et al.[38] and Nakai et al.[39] reported a broad 90° peaking for π^+ emission at $E_\pi^{c.m.} \simeq 10$-20 MeV in

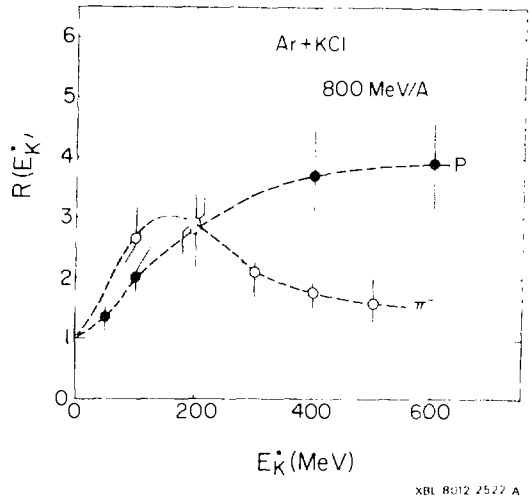

Fig. 22 The 30° to 90° yield ratio in the c.m. frame, plotted as a function of the kinetic energy in that frame.

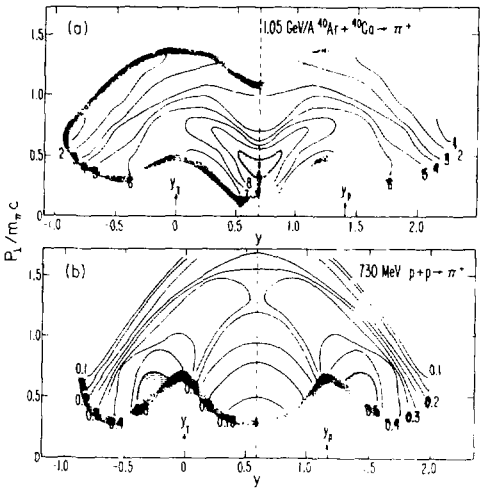

Fig. 23 Data of π^+ by Wolf et al. to show 90° peaking.

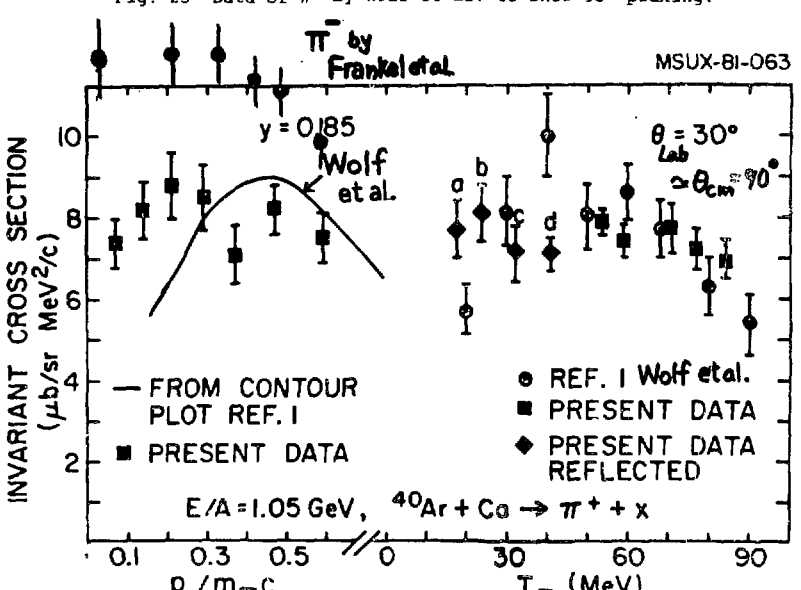

Fig. 24 Preliminary data of π^+ and π^- by Frankel et al. to show no evidence on the 90° peaking.

Ar + Ca and Ne + NaF collisions. The well-known plot for this broad peaking is shown in Fig. 23. Libbrecht and Koonin[40] studied Coulomb effects on pion emission and showed that this broad peaking might be due to the Coulomb foucusing effect. If the Coulomb effect is responsible, then it is rather interesting to measure both π^+ and π^-.

Recently Frankel et al.[41] measured both π^+ and π^- by a magnetic spectrometer in 1.05 GeV/nucleon Ar + Ca collisions, the same projectile and target combinations used by Wolf et al. In Fig. 24 their preliminary data are displayed. In the left-hand side of the figure the p_T distributions of both π^- and π^+ at c.m. 90^o are shown. The yield of π^- is consistently larger than that of π^+, probably because of the Coulomb effect. However, these data do not show any peaking, which strongly contradict the data by Wolf et al. According to Frankel et al., the difference may have originated from the trick of the contour plot, because if they plot the raw data at $\theta_{Lab} = 30^o$ (which roughly corresponds to c.m. 90^o), then their data agree reasonably well with the data by Wolf et al. except for one or two points, as seen in the right-hand side of Fig. 24. However, if the data points are connected by a smooth curve, one set of the data produces a peak while the other set does not. The peaking is anyway about a 20 % effect in the cross section, and the measurements are not easy. We should perhaps wait for another independent experiment to pin down this 90^o puzzle.

6.3. Subthreshold Pion Production

In nucleon-nucleon collisions the threshold energy of pion production is 290 MeV. Therefore, any pion production in nuclear collisions with beams below 290 MeV/nucleon is due to the nuclear effect.

Benenson et al.[42] have measured both π^- and π^+ at 0^o in Ne + NaF collisions and showed that pions are produced even at beam energy of 80

MeV/nucleon, as shown in Fig. 25. For the production of 70-80 MeV pions in the laboratory frame with 80 MeV/nucleon beams, if we ignore Fermi motion, then about 9 nucleons have to sum their kinetic energies to create one pion, because in the c.m. frame the kinetic energy plus rest mass of these pions is about 185 MeV while the beam energy per nucleon in this frame is only 20 MeV/nucleon. If these pions are created in single nucleon-nucleon collisions, then we have to assume a Fermi motion of about 400 MeV/c.

Subthreshold pion production has also been studied at c.m. 90° in 200 MeV/nucleon Ne + NaF collisions.[43] Very preliminary data are shown in Fig. 26 (The absolute value is reliable only within a factor of 2-3). In the c.m. frame the kinetic energies of the observed pions extend up to 260 MeV. For the production of such high energy pions about 8 nucleons have to sum their kinetic energies. This situation is very similar to the case studied just above for 0° pion production by 80 MeV/nucleon beams. However, if we

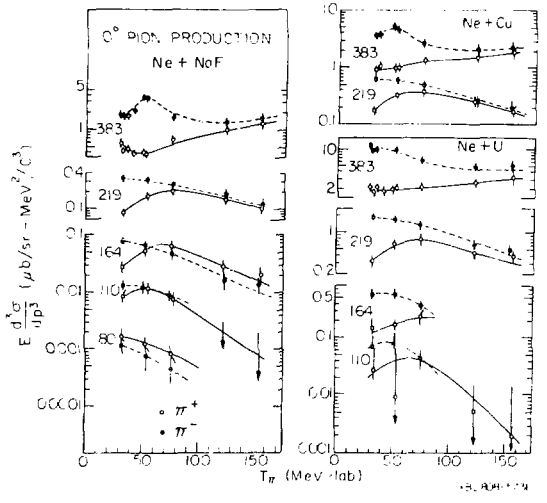

Fig. 25 Pion production at 0° with low energy beams.

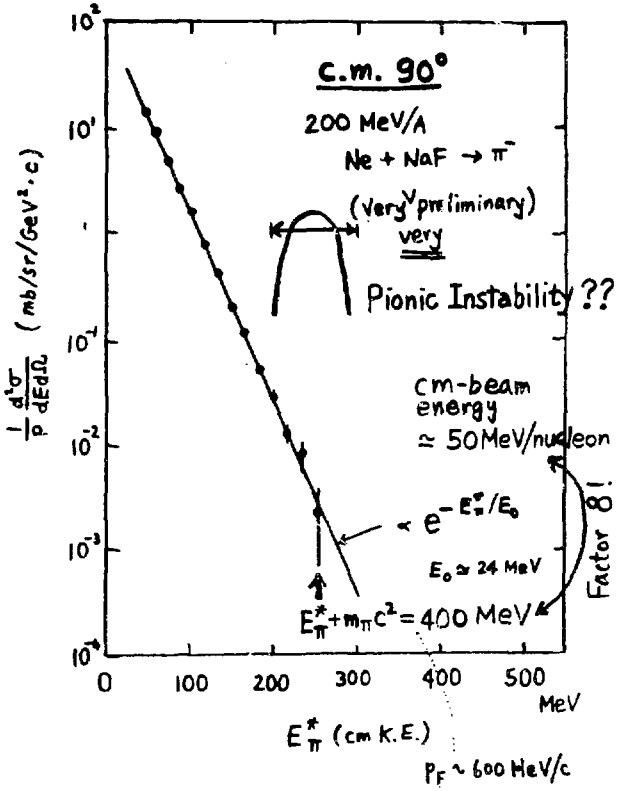

Fig. 26 Pion production at 90° with 200 MeV/nucleon beams. Data are very preliminary.

look at the data more carefully we notice that the cross section to produce 260 MeV pions (in the c.m.) as seen in Fig. 26 is about 1000 times smaller than the cross section to produce pions at 0° with 80 MeV/nucleon beams. This is an interesting aspect. In terms of single nucleon-nucleon collisions we need 600 MeV/c Fermi motion in the former case while 400 MeV/c in the latter. This fact may perhaps be responsible for creating such a large difference in cross sections. Another interesting aspect seen in Fig. 26 is that the energy spectrum is almost of a pure exponential type down to such low cross sections.

This is rather surprising.

SUMMARY:

1. The average pion multiplicity $\langle m_\pi \rangle$ is proportional to $P^{2/3}$ where P is the average nucleon number in the participant region. This fact suggests the importance of pion absorption process.
2. Energy spectra in the c.m. frame are almost exponential at any angle and at any beam energy.
3. At 1 GeV/nucleon beam energies the angular distribution in the c.m. frame shows forward peaking at $E_\pi^{c.m.} \approx 150$ MeV, presumably due to the formation of Δ. The 90° peaking at $E_\pi^{c.m.}$ is now uncertain.
4. Subthreshold pion production is a useful tool to study energy concentration in high energy nuclear collisions and has been studied at both 0° and c.m. 90°. Pions which require an energy concentration of about 8-9 times the average beam energy per nucleon are observed.
5. Although I have not discussed it, no messages have yet been obtained on the evidence of pion condensation.

7. RATIOS OF π^-/π^+, n/p AND t/^{3}He

7.1. π^- to π^+ Ratio

In Fig. 27 the data of π^- and π^+ measured at 0° in collisions of 380 MeV/nucleon Ne + NaF are displayed. To a first-order approximation we expect that both π^- and π^+ yields should be the same, since both Ne and NaF contain almost equal proton and neutron numbers. However, as seen from the figure, the yields of π^- are much higher than those of π^+. In addition, the yields of π^- have a sharp peak at a certain momentum, whereas those of π^+ have a valley there. The pion velocity at this peak (or valley) is very close to the beam velocity which is indicated by an arrow in Fig. 27. The ratio of π^- to π^+

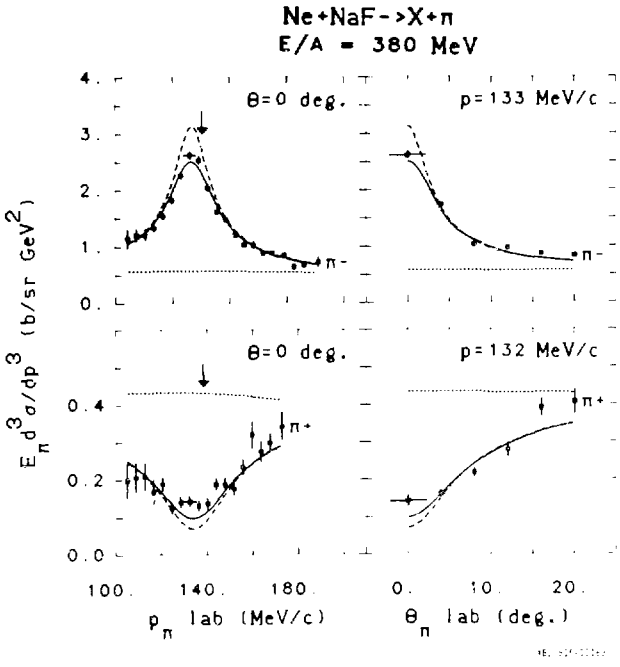

Fig. 27 Spectra of π^- and π^+ emitted at forward angles.

there reaches about 20-30.

It is expected that projectile fragments are clustered dominantly at 0° at the beam velocity. Since these clusters carry positive charges, negative pions produced in the collisions will be attracted by these clusters due to Coulomb interactions, whereas positive pions will be repelled from them. Therefore, we expect large yields of π^- and small yields of π^+. In fact, theoretical calculations of Coulomb interactions[40,44] explain reasonably well these observed features.

Although it is expected that Coulomb effects are the strongest at 0°, it is also interesting to study how these effects appear in the data at large

angles. In Fig. 26 the π^- to π^+ ratios measured at 30°, 60°, and 90° are plotted as a function of the measured pion momentum for various collisions at beam energies of 800 MeV/nucleon. In the Ne + NaF case the ratio is larger than one only in the small momentum region at 30°, while it is close to one at 60° and 90° for all momenta. A similar tendency is observed for Ar + KCl. These facts imply that the Coulomb effects are anisotropic in the laboratory frame and are stronger at smaller angles. This is consistent with the expectation that most of the nuclear charges are clustered along the beam axis. For Ar + Pb stronger Coulomb effects are observed mainly because of the larger nuclear charge of the system.

Detailed study of Coulomb effects may tell us useful information on the nuclear transparency. If the nucleus is completely transparent, then both projectile and target pass through each other, and consequently, most of nuclear charges are clustered at $(y,p_T) = (y_p,0)$ and $(y_T,0)$. On the other

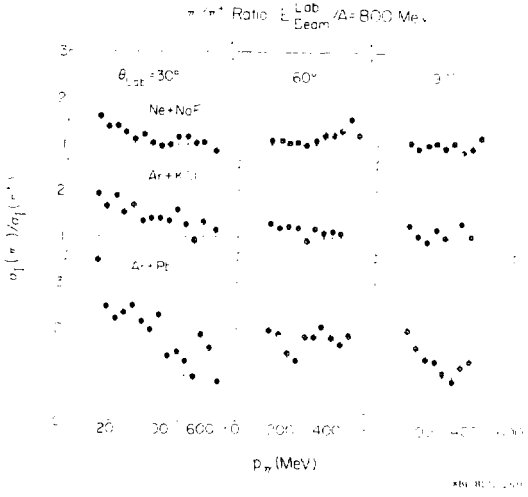

Fig. 28 Ratios of π^- to π^+ at large angles.

hand, if the nucleus is completely black, then the projectile and target stop each other completely in the c.m. frame. A theoretical value of the π^- to π^+ ratio at $p_T = 0$ at c.m. 90^o for Ar + KCl collisions (at around 1 GeV/nucleon) is 2.8 for the complete black case and 1.6 for the complete transparent case.[45] The observed value is about 2 which is in between the two extreme cases.

7.2. Neutron to Proton and Triton to ^{3}He Ratios

If π^- to π^+ ratios show Coulomb effects, we expect also that the neutron to proton as well as the triton to ^{3}He ratios should be affected by Coulomb

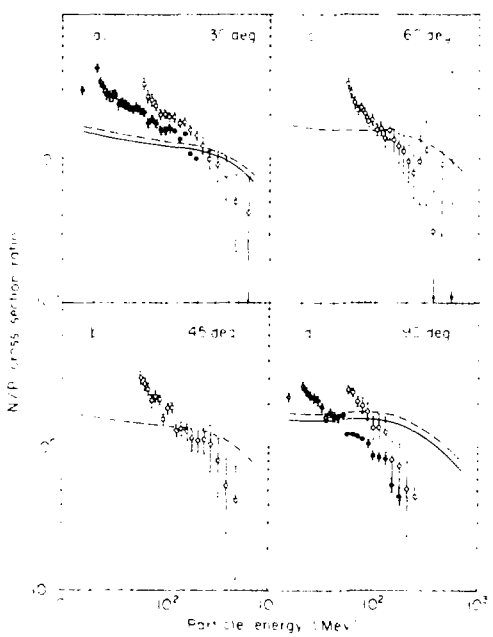

Fig. 29 Neutron to proton ratios measured in Ne + (U,Pb) collisions.

interactions. In Fig. 29 the observed neutron to proton ratios[46] in 300-400 MeV/nucleon Ne + (Pb,U) collisions are displayed. Unfortunately these neutron and proton measurements were done at slightly different beam energies. Nevertheless, we clearly observe that the n/p ratio is larger at smaller fragment energy. A similar tendency is observed in the data of triton to ^{3}He,[10] as shown in Fig. 30.

These facts immediately suggest that Coulomb effects may also be important in explaining the observed n/p and t/^{3}He ratios. However, if we compare the observed momentum dependence of the n/p or t/^{3}He ratio with the π^-/π^+ ratio, we notice that the mechanism which causes an enhancement in the ratio in the small momentum region may not be necessarily the same. For example, in the case of π^- to π^+, the ratio is larger than the N/Z of the system (N: neutron number, Z: proton number) in the small momentum region at forward angles but not at large angles (Fig. 28), whereas such a large ratio

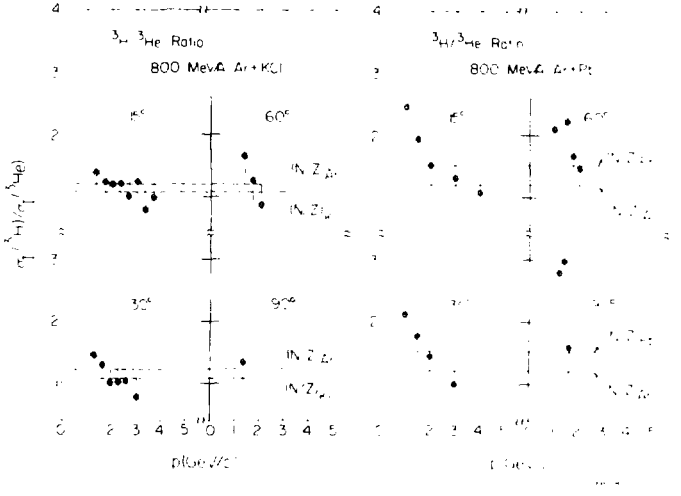

Fig. 30 Triton to ^{3}He ratios in Ar + KCl and Pb collisions.

is observed at all angles in the case of n/p and t/^{3}He ratios (Figs. 29 and 30).

For a system with N/Z > 1, such as Ne + Pb, one would naively expect that a different mechanism might be involved in the case of the n/p or t/^{3}He ratio as compared to the π^-/π^+ ratio. The neutron to proton ratio for the originally produced nucleons (in the sense of cascade calculations) would be almost equal to the N/Z ratio of the system. However, some of these nucleons will be combined to form composite fragments before they are actually emitted. Among them the deuteron emission would be the largest. Since deuterons carry equal numbers of protons and neutrons, the remaining neutrons and protons might form a ratio which is much larger than the N/Z ratio of the system. This idea has theoretically been formulated by Randrup and Koonin[47] and also by Stevenson[48] in order to explain the observed neutron to proton ratios. According to them, a large ratio is expected in the small momentum region at all angles because deuterons are more easily produced there. In fact, Stevenson showed that this effect without any Coulomb effect already explains the major feature of the data of the n/p ratio shown in Fig. 29. Therefore, a careful treatment is required when one applies the theory of Coulomb effects on the ratios of n/p and t/^{3}He.

SUMMARY:

1. The cross section of π^- has a sharp peak at 0° at the beam velocity and that of π^+ has a valley there. This fact strongly suggests that Coulomb interactions distort pion spectra especially at the region of the beam velocity.
2. At large laboratory angles the π^- to π^+ ratio is larger than the N/Z ratio of the system especially in the small momentum region at forward angles.
3. The n/p and t/^{3}He ratios are larger than the N/Z ratio of the system in the small momentum region at all angles. Coulomb effects as well as other

mechanisms, such as isospin equilibration, must be considered in order to explain these ratios.

8. PRODUCTION OF STRANGE PARTICLES

In Fig. 31 various threshold energies for particle production in nucleon nucleon collisions are listed. At around 2 GeV the threshold energies for the production of strange particles are clustered. In this talk I will discuss K^+ and Λ.

The motivation of measuring K^+ or Λ is as follows. Since the cross section of $K^+ + N$ [$\sigma(K^+N) \approx 10$ mb] is much smaller than that of $N + N$ [$\sigma(NN) \approx 40$ mb] or $\pi + N$ [$\sigma(\pi N) \approx 200$ mb], K^+ is less likely to be rescattered by

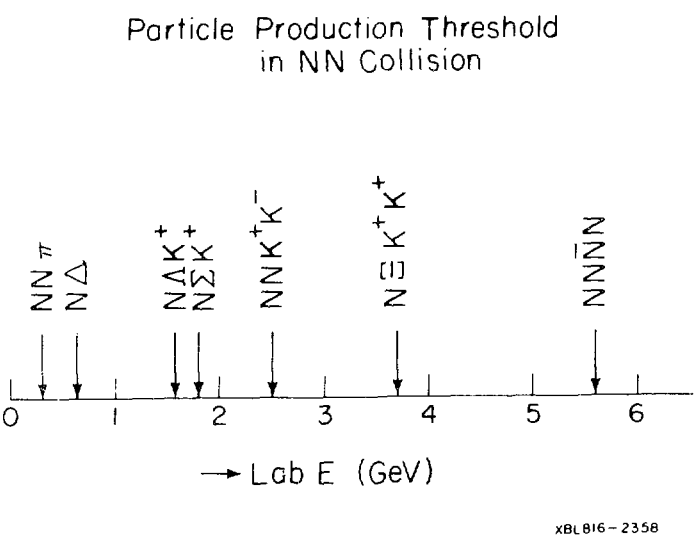

Fig. 31 Particle production threshold energies in nucleon nucleon collisions.

surrounding nucleons (compared to π^- or N), and thus reflects more of the features of the violent stage of the collision at which particles are created. In addition, because of the strangeness conservation, K^+ is less likely absorbed inside the nucleus. These situations for K^+ production are quite different from those for pions.

Schnetzer et al.[49] have measured K^+ spectra and its associate multiplicity with a magnetic spectrometer and 16 multiplicity counters. In Fig. 32 an example of the measured energy spectrum in the c.m. frame is plotted for 2.1 GeV/nucleon Ne + NaF collisions. The spectrum shape is almost exponential with the inverse exponential slope, E_0, around 142 MeV. If this

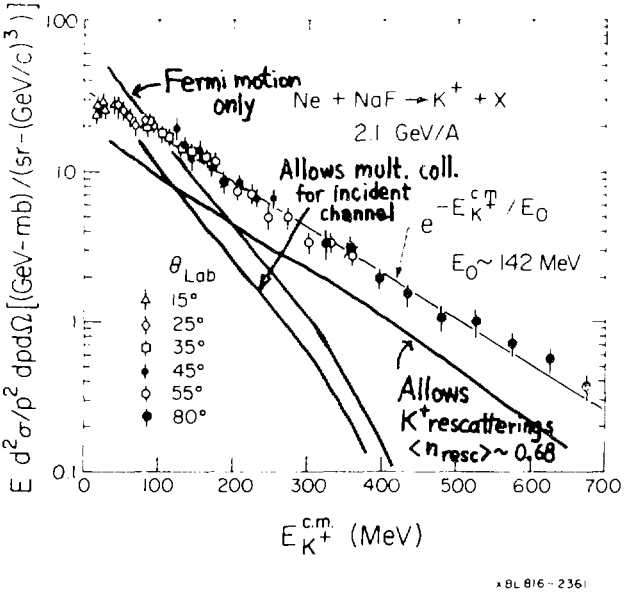

XBL 816-2361

Fig. 32 The K^+ spectrum in 2.1 GeV/nucleon Ne + NaF collisions.

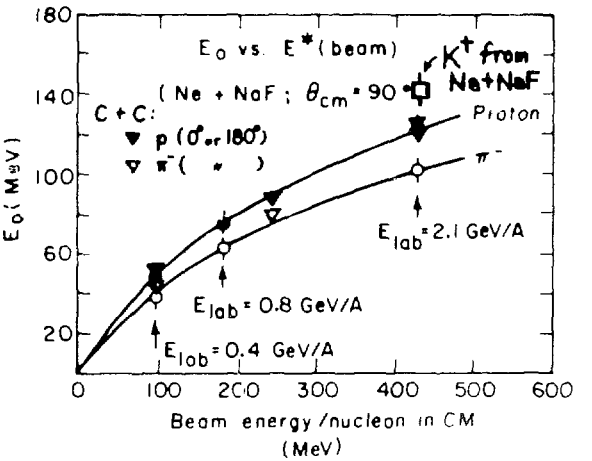

Fig. 33 Observed E_0 for K^+ as compared with E_0 for protons and pions.

E_0 is plotted on the same graph shown before, then the value of E_0 for K^+ is much larger than E_0 for protons of pions (see Fig. 33). This fact implies that K^+ reflects more violent stage than protons and pions do.

Then how much useful information can we obtain from the kaon spectra? In order to create 0.7 GeV (kinetic energy) K^+ in the c.m. frame by a single nucleon-nucleon collision, one needs a Fermi motion of 7~800 MeV/c which is unrealistically too large for one nucleon to carry. Therefore, one can have a strong hope that the cumulative effect can most sensitively be studied from the K^+ spectrum.

However, the actual situation is rather complicated. According to Randrup and Ko[50], the data are, in fact, not explained by Fermi motion only. Also, it is not possible to reproduce the data even if the multiple collisions for the incident channel are taken into account. However, if we allow slight

rescatterings of K^+ after its creation, for example, at the level of an average number of rescattering of 0.68, then such rescatterings broadens the spectrum up to the observed slope, as seen in Fig. 32. This is somewhat discouraging. Nature is not always kind when we strive for a new physics.

The projectile and target mass dependences of the K^+ production has also been studied by Schnetzer et al. The data shows that

$$\sigma \propto A_p \times A_T, \tag{23}$$

where A_p and A_T are the projectile and target mass numbers respectively. This relation is somewhat different from that expected by a simple participant-spectator model in which we have $A_p A_T^{2/3} + A_T A_p^{2/3}$. The above relation, Eq. (23), is consistent with the prediction by Randrup and Ko.

We should also mention the thermal model. If we assume chemical equilibrium, then a calculation showed a factor of 20 larger yield than the data, although the shape of the momentum spectra as well as the angular distributions are reasonably well reproduced.[51]

The Λ production has been studied recently by Harris et al.[52] with a streamer chamber in 1.8 GeV/nucleon Ar + KCl collisions. In this measurement the decay of Λ,

$$\Lambda \rightarrow p + \pi^- \quad (64\ \% \text{ branching}), \tag{24}$$

was used for the identification. A plot of the measured invariant mass for the $p\pi^-$ system is shown in Fig. 34. We clearly observe the signal of Λ.

In Fig. 35 the observed momentum distribution of Λ is plotted in the plane of the parallel and transverse momenta in the c.m. frame. The circle in the figure indicates the expected kinematical region for Λ production in 1.8

GeV nucleon + nucleon collisions. Most of the observed points are scattered outside this nucleon-nucleon kinematical limit. Very few points inside this circle are somewhat inconsistent with the previous K^+ data, but it is consistent with the K^+ data that the observed points are scattered over a wide kinematical region.

I would like to mention here one interesting aspect of Λ production. Since the decay of Λ shown in Eq. (24) is via weak interactions, the angular distribution of p or π^- is not isotropic if Λ has a polarization. In general, the angular distribution of p or π^- with respect to the polarization axis of Λ is given by

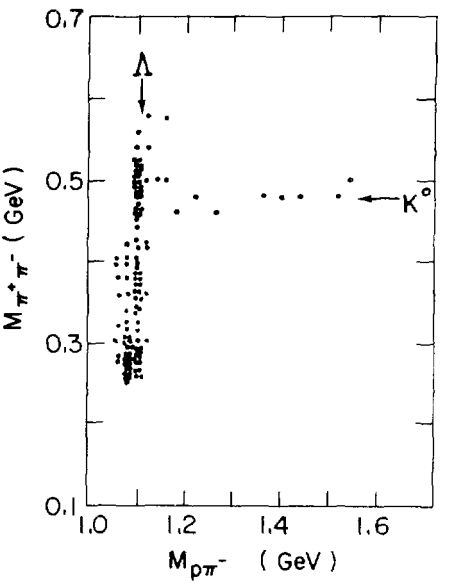

XBL 804-753

Fig. 34 Invariant mass plot for positive + negative charged particles.

$$W(\theta) = 1 + \alpha P \cos\theta, \qquad (25)$$

with α in this case is -0.64. By defining the reaction plane such that the beam and the emitted Λ form this plane, Harris et al. determined the polarization, P, to be

$$P = -0.10 \pm 0.05. \qquad (26)$$

So far, inclusive measurements have neglected the quantity of angular momentum or spin, but such a variable is extremely interesting measurement for the future.

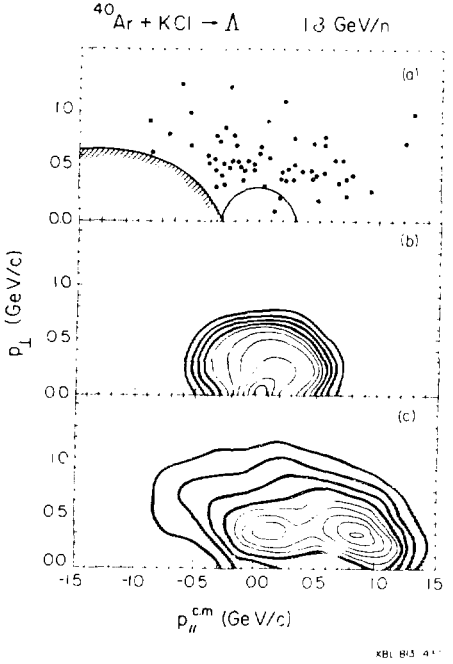

Fig. 35 Distribution of the observed Λ particles in the c.m. momentum space (top figure). Circle indicate the kinematical limit in nucleon nucleon collisions.

SUMMARY:

1. Production of K^+ or Λ has recently been observed. Especially for K^+ the observed spectrum is almost exponential with the inverse slope E_0 being larger than the corresponding values for protons and pions.
2. The cross section of the K^+ production is approximately proportional to $A_P \times A_T$, where A_P and A_T are, respectively, the projectile and target mass numbers.
3. In terms of the quark model K^+ and Λ are described as $(u\bar{s})$ and (uds), respectively. Strange quarks have to be created to produce these particles. Especially for Λ, spins of u and d are coupled to zero,[53] and therefore the polarization of Λ readily measures the polarization of the s-quark. Measurements of Λ polarization is thus interesting and perhaps useful for a study of the roles of quarks in high energy nuclear collisions.

9. PHYSICS RELATED TO PROJECTILE FRAGMENTS

From the viewpoint of the study of the collision mechanism the spectator region seems to be less interesting, because it is the region where no strong nucleon-nucleon collisions take place. However, several interesting physics phenomena are hiding in this region, and perhaps, this region will supply one of the most promising futures of high-energy nuclear collisions. I select two topics related to the projectile fragments; the high momentum component of nucleons inside the nucleus and the production of neutron-rich isotopes.

9.1. High Momentum Component inside the Nucleus

Since the projectile fragment is formed from a cluster which has not experienced any strong interaction, it tends to keep the various static properties that the projectile nucleus had before the collision. Recently

Fujita, Hüfner, and Nemes[54,55] pointed out that the parallel momentum distribution in the the fragmentation process of the one-nucleon removal reaction, such as $\alpha \rightarrow {}^{3}He$ or ${}^{16}O \rightarrow {}^{15}O$, will directly reflect the internal motion of nucleons inside the nucleus. In high energy nuclear collisions the momentum transfer, $\vec{q}$, in the process of projectile fragmentation is much smaller than the original projectile momentum, $\vec{P}_{Beam}$, since $|\vec{q}| \approx \hbar/R \approx$ (a few 100) MeV/c while $|\vec{P}_{Beam}| >$ 10 GeV/c. We therefore expect that $\vec{q} \perp \vec{P}_{Beam}$. In other words, the transverse momentum distribution of fragments may contain both the effects of the nuclear reaction and the internal motion, whereas the longitudinal momentum distribution tends to reflect only the internal motion.

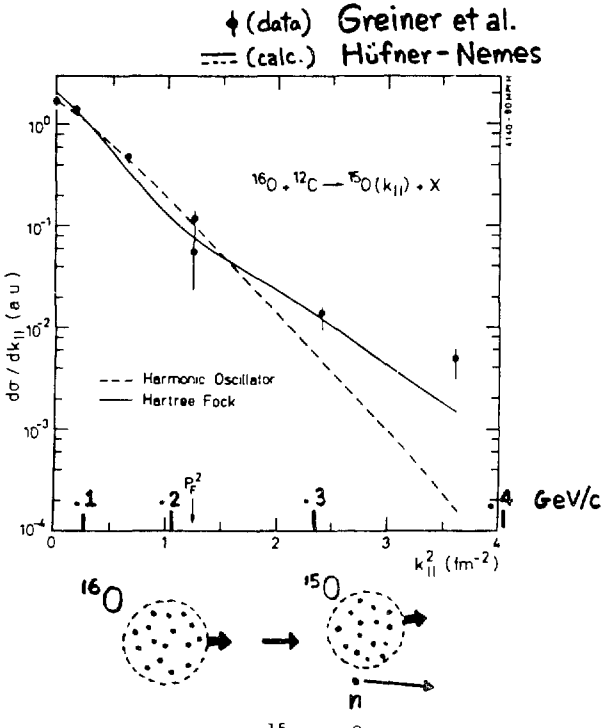

Fig. 36 Momentum distribution of ^{15}O at 0^{o} in the projectile rest frame.

The one-nucleon removal reaction has a further merit for the study of the internal motion of nucleons. This reaction is an almost exclusive reaction, because if one takes out (A-1) cluster from A, then only one nucleon is left over which was scraped out by the target. From momentum conservation, therefore, the longitudinal momentum distribution of the observed (A-1) cluster in the projectile rest frame would immediately reflect the momentum distribution of the single nucleon (which was scraped out by the target) inside the projectile nucleus. In Fig. 36 the data by Greiner et al.[56] for the process of $^{16}O \rightarrow {}^{15}O$ are shown. Hüfner et al. concluded that a simple Gaussian momentum distribution of a single nucleon inside the nucleus does not explain the data and suggested that an appropriate modification of the nuclear wavefunction is required in the high momentum region. This analysis neglects multi-step processes in creating the observed ^{15}O, and perhaps needs a more careful consideration. But, I think that it is quite interesting and important to extend such measurements into a much higher momentum region.

9.2. Production of Neutron Rich Isotopes

The second interesting subject for projectile fragments is the production of neutron rich isotopes. To a first order approximation, the neutron to proton ratio (N/Z ratio) of the projectile spectator is nearly equal to the N/Z ratio of the projectile nucleus, since the former is a part of the latter. For example, if we use ^{238}U as a projectile, then $N/Z = 1.6$. It is well known that the stability line of the nucleus extends along $N = Z$ for light nuclei, and thus the projectile spectators from U beams tend to fill the unstable neutron-rich-isotope region. Of course, the N/Z ratio of the detected projectile fragment is not really the same as that of the projectile spectator because of the the existence of the evaporation process (ablation) which occurs after the scraping process of the projectile nucleus by the target

(abrasion).[57,58] However, the important point here is that the neutron rich isotopes are rather easily produced by using high-energy nucleus beams.

So far, three sets of experimental data[59-61] have been reported on the discovery of new neutron rich isotopes. Symons et al.[59] and Westfall et al.[60] have accelerated ^{40}Ar and ^{48}Ca beams and discovered 16 new isotopes, as shown in Fig. 37. This type of study will open up a variety of new applications of high energy nucleus beams, especially if we have U beams. Is there a new region of stability? How about a new region of deformation? Is the proton radius significantly different from the neutron radius? How about static properties of new isotopes, such as lifetimes or magnetic moments? Are there any polarization or alignment associated with the isotope production? These are some of a number of interesting questions.

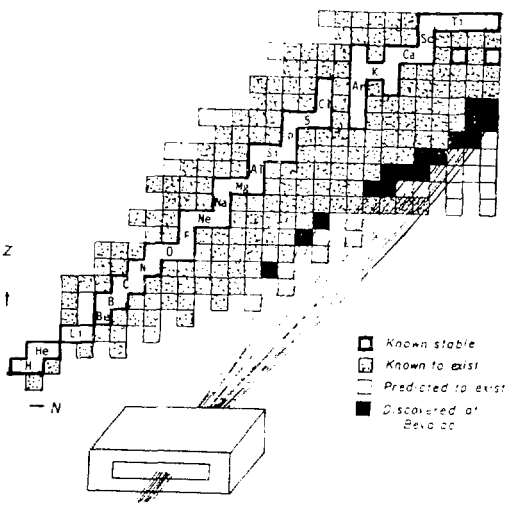

Fig. 37 New isotopes produced by ^{40}Ar and ^{48}Ca beams

Another interesting application of neutron rich isotopes is their use as secondary beams. Because projectile fragments have their velocity which is almost equal to the projectile velocity, we may have a chance to use them as secondary beams. So far, only stable nuclei were used as projectiles, but in the future, we may be able to use unstable nuclei as projectiles. For example, if U beams become available, it may be possible to use ^{52}Ca as a projectile. I think we should pursue this rather seriously.

In connection with neutron rich isotopes I would like to mention another interesting result. Moeller et al.[62] have recently measured the cross

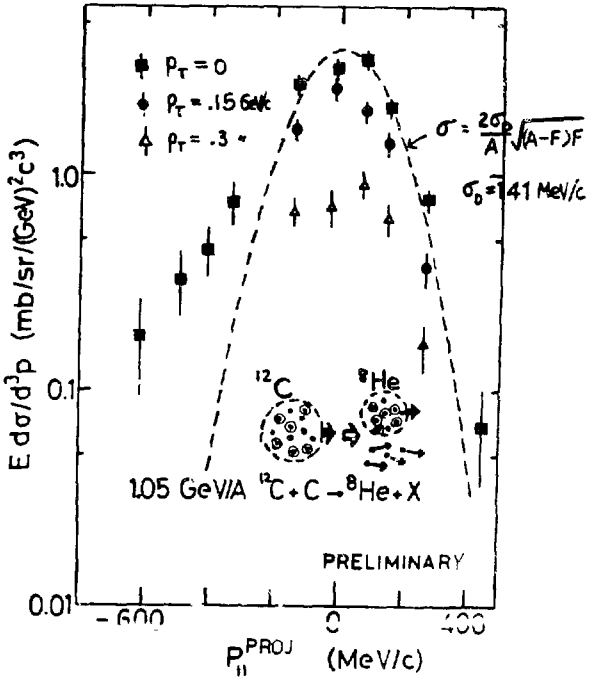

Fig. 38 Production of ^{8}He at 0° in C + C collisions.

sections of ^{8}He production in 2.1 GeV/nucleon C + C collisions, as shown in Fig. 38. In this case, four protons are scraped out from the projectile carbon nucleus, and it is a quite interesting process from the viewpoint of the reaction mechanism. The production cross section is about 35 μb which is about 30 time larger than the production cross section of ^{8}He as a target fragment in collisions of 2.2 GeV p + C (1.2 μb).[63] Using current theories it is very hard to explain such a large discrepancy, and it may be an interesting subject to be studied in the future.

SUMMARY:

1. It is useful to study the parallel momentum distribution in the one nucleon removal reaction for the purpose of studying the nucleon momentum distribution inside the static nucleus. Using an electron machine it is rather hard to extract the internal momentum which is larger than 0.3 GeV/c. High energy nucleus beams may offer a unique opportunity for the study of internal momentum distribution.
2. Production of neutron rich isotopes may open up a variety of future applications of high energy nucleus beams. Many topics can be studied in relation to these neutron rich isotopes.
3. I would like to emphasize again the future usage of neutron rich isotopes as secondary beams.

10. SUMMARY

Let me summarize my talk. Because I already listed a summary for each individual topic at the end of each section, I would like to summarize the whole talk from a somewhat different viewpoint.

At a beam energy of around 1 GeV/nucleon the de Broglie wave length of the incident nucleons inside the projectile ($\lambda_{\text{de Broglie}} \approx 0.3$–$0.5$ fm) is much

shorter than the typical internucleon separation (d ≃ 1.8 fm) inside the nucleus. This fact implies that nucleons inside the projectile nucleus can recognize the individuality of nucleons inside the target nucleus. Therefore, to a first order approximation, the high energy nucleus beam is a simple assembly of nucleon beams.

Then, what is the uniqueness of the nucleus-nucleus collision as compared with the nucleon-nucleon collision. The first obvious feature of the nucleus beam is the clustering of nucleons inside the projectile nucleus (see the upper half of Fig. 39). For a projectile with a mass number of 40-50, there are about 10 nucleons/(a few fm)^2 ≃ 10^{26} nucleons/cm^2, and this nucleon

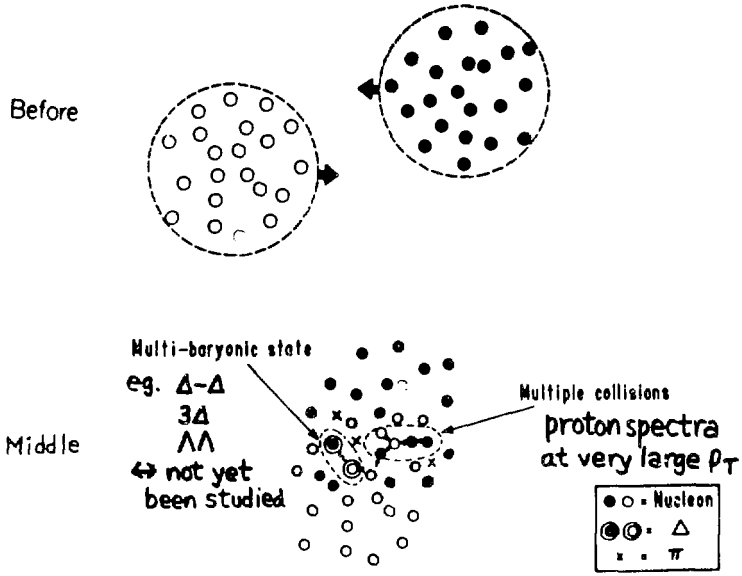

Fig. 39 Features of nuclear collisions (I).

beam is also sharply bunched in time; a few nucleons per t = (a few fm)/c ≃ 10^{-23} s. As a result, the product of these two numbers leads to an instantaneous flux of about $10^{49}/cm^2/s$, which cannot be obtained by any conventional proton accelerator. Thus, the nucleus beam may be regarded as a locally high flux nucleon beam.

The clusterization of nucleons induces several effects that are unique to high-energy nuclear collisions. During the course of a collision we have multiple nucleon-nucleon collisions, as shown in the lower half of Fig. 39. Macroscopically, these multiple collisions are a very important process for creating high density, and thus it is essential to study where we can more sensitively observe such a process. The importance of this process has been studied, in this talk, especially for large p_T proton emission in Sec. 4. At a beam energy of around 1 GeV/nucleon we also expect a copious production of Δ particles. These Δ particles may interact with each other to create multi baryonic excited states, such as Δ-Δ or 3Δ state. Specifically, a possibility to form a Δ-Δ bound state has theoretically been studied in the past.[64-66] This multi-baryonic excited state is a very interesting subject to be studied in the future.

After the collision we expect the following situation as illustrated in Fig. 40. Two groups of nucleons which have not experienced any hard nucleon-nucleon collision will be created. These two groups are called the projectile and target spectators, respectively, and they produce projectile and target fragments. Nucleons which have experienced hard nucleon-nucleon collisions are scattered out at all angles, and are called the participant. In this talk the usefulness of this participant-spectator model has been studied especially from the total integrated cross sections of nuclear charge or mass in Sec. 3.

Some of the participant nucleons may stick together to form a composite particle. We studied the formation mechanism of composite fragments in Sec.

5. Also, from the composite spectra the radius of the participant region has been estimated to be 2-3 fm.

Pions are also created. We have studied in Sec. 6 that some pions are absorbed, as shown in the Fig. 40, by surrounding nucleons. Some pions experience large Coulomb forces which induce a large π^-/π^+ ratio, as studied in Sec. 7.

Although the production cross section of strange particles are small, we have seen K^+ or Λ in Sec. 8. These particles have relatively long mean free paths and thereby less likely be rescattered as also shown in Fig. 40.

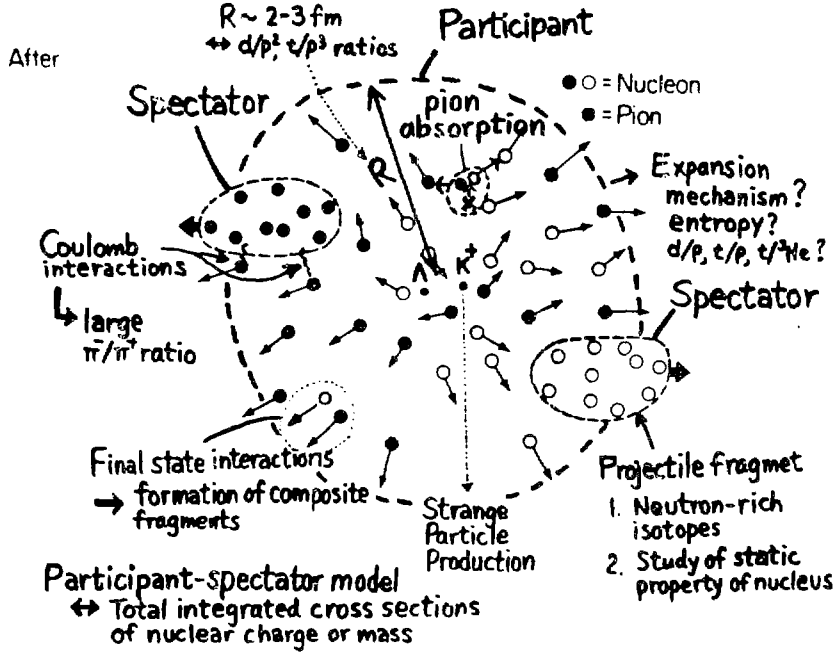

Fig. 40 Features of nuclear collisions (II).

One of the interesting questions related to the participant region is how the whole system expands after the collision. The quantity of entropy is certainly an interesting one which is related to the macroscopic expansion mechanism, but I feel that we need a more careful work here. Also, it is certainly an interesting question to study if d/p, t/p, or $t/^3He$ ratios are related to the macroscopic expansion mechanism.

With regard to the spectator, we have learned in Sec. 9 that the projectile fragment may be a useful probe to study the internal motion of clusters inside the static nucleus. In addition, we learned that the neutron rich isotopes will open up a variety of future applications.

I think that the physics learned from inclusive spectra are more or less displayed in these two figures; in Figs. 39 and 40, and particularly in the latter.

So far, nothing exotic have been observed in the inclusive data. However, the inclusive data have been (and still are) very useful in studying the actual reaction mechanism of the complicated nucleus-nucleus collision. As I mentioned in Sec. 2, the available data cover only a small portion of the kinematical area allowed by the collision kinematics. In the future it is definitely important to measure inclusive spectrum in such an unmeasured region. Theoretically, no satisfactory explanations have yet been available for most of the data shown in this talk. Therefore, my final conclusion is that both experimental and theoretical studies of inclusive spectra must still to be done in the future.

ACKNOWLEDGMENTS

In this talk I used a number of unpublished data. First of all I would like to thank L. Anderson, S. Chessin, K. Frankel, C. Celbke, J. Harris, E.

Moeller, A. Sandoval, L. Schroeder, J. Sullivan, and J. O. Rasmussen for their permission to use their data prior to the publication. My thanks also extend to our collaborators, L. Anderson, Xi-Xiang Bai, O. Chamberlain, H. Hamagaki, O. Hashimoto, S. Kadota, M.-C. Lemaire, R. Lombard, Y. Miake, E. Moeller, K. Omata, S. Schnetzer, G. Shapiro, Y. Shida, H. Steiner, and I. Tanihata, for stimulating daily discussions. Special thanks are due to S. Bohrmann for his calculations, shown in Fig. 8, for the purpose of this talk. This work is supported by the Director, the Office of Energy Research, Division of Nuclear Physics of the Office of High-Energy and Nuclear Physics of the U.S. Department of Energy under Contract W-7405-ENG-48. It is also supported by the INS LBL Collaboration Program and a grant from the Commemorative Association of the Japan World Exposition.

REPERENCES

1. This streamer chamber picture was taken at the Bevalac by the UC-Riverside group in 1.8 GeV/nucleon Ar + Pb collisions.
2. Both adages came from the Analects of Confucius in China. However, currently the first one is more frequently used in Japan and the second one in China.
3. J. D. Bowman, W. J. Swiatecki, and C. F. Tsang, Lawrence Berkeley Laboratory Report LBL-2908 (1973), unpublished.
4. R. J. Glauber and G. Matthiae, Nucl. Phys. B21, 135 (1970).
5. J. Hüfner and J. Knoll, Nucl. Phys. A290, 460 (1977); also see J. Hüfner, in Proc. 4th High-Energy Heavy-Ion Summer Study, Berkeley, 1978, LBL-7766, p. 135.
6. S. Nagamiya, Nucl. Phys. A335, 517 (1980).
7. P. J. Lindstrom, D. E. Greiner, H. Heckman, B. Cork, and F. S. Bieser, Lawrence Berkeley Laboratory Report LBL-3650 (1975), unpublished.
8. D. J. Morrissey, W. Loveland, M. de Saint Simon and G. T. Seaborg, Lawrence Berkeley Laboratory Report LBL-8983 (1979).
9. S. B. Kaufman, M. W. Weisfield, E. P. Steinberg, B. D. Wilkins and D. Henderson, Phys. Rev. C14, 1121 (1976).
10. S. Nagamiya, M.-C. Lemaire, E. Moeller, S. Schnetzer, G. Shapiro, H. Steiner, and I. Tanihata, Phys. Rev. C (in press) [Preprint, Lawrence Berkeley Laboratory Report LBL-12123 (1981)].
11. G. D. Westfall, J. Gosset, P. J. Johansen, A. M. Poskanzer, W. G. Meyer, H. H. Gutbrod, A. Sandoval, and R. Stock, Phys. Rev. Lett. 37, 1202 (1976).
12. J. Gosset, H. H. Gutbrod, W. G. Meyer, A. M. Poskanzer, A. Sandoval, R. Stock, and G. D. Westfall, Phys. Rev. C16, 629 (1977).

13. S. Nagamiya, L. Anderson, W. Bruckner, O. Chamberlain, M.-C. Lemaire, S. Schnetzer, G. Shapiro, H. Steiner, and I. Tanihata, Phys. Lett. 81B, 147 (1979).

14. A. Sandoval, H. H. Gutbrod, W. G. Meyer, R. Stock, Ch. Lukner, A. M. Poskanzer, J. Gosset, J.-C. Jourdain, C. H. King, G. King, Nguyen Van Sen, G. D. Westfall, and K. L. Wolf, Phys. Rev. C21, 1321 (1980).

15. J. V. Geaga, S. A. Chessin, J. Y. Grossiord, J. W. Harris, D. L. Hendrie, L. S. Schroeder, R. N. Treuhaft, and K. Van Bibber, Phys. Rev. lett. 45, 1993 (1981).

16. S. Bohrmann, private communication (1981).

17. I. Tanihata, M.-C. Lemaire, S. Nagamiya, and S. Schnetzer, Phys. Lett. 97B, 363 (1980).

18. I. Tanihata, S. Nagamiya, S. Schnetzer, and H. Steiner, Phys. Lett. 100B, 121 (1981).

19. J. I. Kapusta, Phys. Rev. C21, 1301 (1980).

20. W. D. Myers, Nucl. Phys. A296, 177 (1978).

21. J. Gosset, J. I. Kapusta, and G. D. Westfall, Phys. Rev. C18, 844 (1978).

22. S. F. Butler and C. A. Fearson, Phys. Rev. 129, 836 (1963).

23. A. Schwarzschild and Č. Zupančič, Phys. Rev. 229, 854 (1963).

24. H. H. Gutbrod, A. Sandoval, P. J. Johansen, A. M. Poskanzer, J. Gosset, W. G. Meyer, G. D. Westfall, and R. Stock, Phys. Rev. Lett. 37, 667 (1976).

25. M.-C. Lemaire, S. Nagamiya, S. Schnetzer, H. Steiner, and I. Tanihata, Phys. Lett. 85B, 38 (1979).

26. A. Z. Mekjian, Nucl. Phys. A312, 491 (1978); Phys. Rev. Lett. 38, 604 (1977); Phys. Rev. C17, 1051 (1978).

27. H. Sato and K. Yazaki, Phys. Lett. 98B, 153 (1981).

28. P. J. Siemens and J. I. Kapusta, Phys. Rev. Lett. 43, 1486 (1979); 43,

1690 (1979) (E).

29. G. Bertsch, Invited Talk presented in this Conference.

30. H. Stöcker, Contributed Paper presented in this Conference. Also, see H. Stocker, Lawrence Berkeley Laboratory Report LBL-12302 (1981).

31. I. N. Mishustin, P. Myhrer, and P. J. Siemens, Phys. Lett. 95B, 361 (1980).

32. C. K. Gelbke, private communication (1981).

33. R. Bond, P. J. Johansen, S. E. Koonin, and S. Garpman, Phys. Lett. 71B, 43 (1977).

34. I learned the idea to relate $\langle m_\pi \rangle$ with P^* in the talk by I. Otterlund; I. Otterland, Invited Talk repended at the Workshop on Future Relativistic Heavy Ion Experiments, GSI, Darmstadt, October 7-10, 1980.

35. R. L. Hatch and S. E. Koonin, Phys. Lett. 81B, 1 (1978).

36. The plot of E_0 for protons and pions at 180° was given by J. V. Geaga and L. S. Schroeder, private communication (1981).

37. L. Anderson, W. Brückner, O. Chamberlain, E. Moeller, S. Nagamiya, S. Nissen-Meyer, D. Nygren, L. Schroeder, S. Schnetzer, G. Shapiro, H. Steiner, and I. Tanihata, Contributed Paper to this Conference and also private communication (1981).

38. K. L. Wolf, H. H. Gutbrod, W. G. Meyer, A. M. Poskanzer, A. Sandoval, R. Stock, J. Gosset, C. H. King, G. King, Nguyen Van Sen, and G. D. Westfall, Phys. Rev. Lett. 42, 1448 (1979).

39. K. Nakai, J. Chiba, I. Tanihata, M. Sasao, H. Bowman, S. Nagamiya, and J. O. Rasmussen, Phys. Rev. C20, 2210 (1979).

40. K. G. Libbrecht and S. E. Koonin, Phys. Rev. Lett. 43, 1581 (1979).

41. K. A. Frankel, J. A. Bistirlich, R. Bossingham, H. R. Bowman, K. M. Crowe, C. J. Martoff, J. Miller, D. L. Murphy, J. O. Rasmussen, J. P. Sullivan, W. A. Zajc, O. Hashimoto, M. Koike, J. Peter, W. Benenson, G.

M. Crawley, E. Kashy, J. A. Nolen, Jr., and J. Quebert, Contributed Paper to this Conference and also private communication (1981).

42. W. Benenson, G. Bertsch, G. M. Crawley, E. Kashy, J. A. Nolen, Jr., H. Bowman, J. G. Ingersoll, J. O. Rasmussen, J. Sullivan, M. Koike, J. Peter, and T. E. Ward, *Phys. Rev. Lett. 43, 683 (1979)*.

43. The data have recently been obtained by us, but the data are extremely preliminaty.

44. M. Gyulassy and S. K. Kauffmann, Nucl. Phys. A362, 503 (1981).

45. M. Gyulassy, private communication, 1981.

46. W. Schimmerling, J. Kast, D. Ortehdahl, R. Madey, R. A. Cecil, B. D. Anderson, and A. R. Baldwin, Phys. Rev. Lett. 43, 1985 (1979).

47. J. Randrup and S. E. Koonin, Nucl. Phys. A356, 223 (1981).

48. J. D. Stevenson, Phys. Rev. Lett. 45, 1773 (1980).

49. S. Schnetzer, M.-C. Lemaire, R. Lombard, E. Moeller, S. Nagamiya, G. Shapiro, H. Steiner, and I. Tanihata, Contributed Paer to 9th International Conference on High Energy Physics and Nuclear Structure, Versailles, July, 1981, also private communication (1981).

50. J. Randrup and C. M. Ko, Nucl. Phys. A343, 519 (1980); also see J. Randrup, Phys. Lett. 99B, 9 (1981).

51. F. Asai, H. Sato, and M. Sano, Phys. Lett. 98B, 19 (1981).

52. J. W. Harris, A. Sandval, R. Stock, H. Stroebele, R. E. Renfordt, J. V. Geaga, H. G. Pugh, L. S. Schroeder, K. L. Wolf, and A. Dacal, Lawrence Berkeley Laboratory Report LBL-12334 (1981).

53. B. Andersson, G. Gustafson, and G. Ingelman, Phys. Lett. 85B, 417 (1979), and references therein.

54. T. Fujita and J. Hüfner, Nucl. Phys. A343, 493 (1980).

55. J. Hüfner and M. C. Nemes, preprint (1981).

56. D. E. Greiner, P. J. Lindstrom, H. H. Heckman, B. Cork, and F. S. Bieser,

Phys. Rev. Lett. 35, 152 (1974).

57. J. Hüfner, K. Schäfer, and B. Schürmann, Phys. Rev. C12, 1888 (1975).

58. D. J. Morrisey, L. F. Oliviera, J. O. Rasmussen, G. T. Seaborg, Y. Yariv, and Z. Fraenkel, Phys. Rev. Lett. 43, 1139 (1979).

59. T. J. M. Symons, V. P. Viyogi, G. D. Westfall, P. Doll, D. E. Greiner, H. Farraggi, P. J. Lindstrom, D. K. Scott, H. J. Crawford, and C. McParland, Phys. Rev. Lett. 42, 40 (1979).

60. G. D. Westfall, T. J. M. Symons, D. E. Greiner, H. H. Heckman, P. J. Lindstrom, J. Mahoney, A. C. Shotter, D. K. Scott, H. J. Crawford, C. McParland, T. C. Awes, C. K. Gelbke, and J. M. Kidd, Phys. Rev. Lett. 43, 1859 (1979).

61. I thought there was a report of new isotopes by plastic detectors, but I cannot find the reference at the moment.

62. E. Moeller, L. Anderson, W. Bruckner, O. Chamberlain, S. Nagamiya, S. Nissen-Meyer, D. Nygren, L. Schroeder, S. Schnetzer, G. Shapiro, H. Steiner, and I. Tanihata, Contributed Paper to this Conference and also private communication (1981).

63. A. M. Poskanzer, R. A. Esterlund, and R. McPherson, Phys. Rev. Lett. 15, 1030 (1965).

64. F. J. Dyson and N.-H. Xuong, Phys. Rev. Lett. 13, 815 (1964).

65. T. Kamae and T. Fujita, Phys. Rev. Lett. 38, 471 (1977).

66. M. Oka and K. Yazaki, Phys. Lett. 90B, 41 (1980).